Sedimentary Geology 424 (2021) 106001

Contents lists available at ScienceDirect

Sedimentary Geology

journal homepage: www.elsevier.com/locate/sedgeo

Bed-scale vertical and lateral distribution of massive sandstone in a topographically confined basin (Peïra Cava, SE France): Implications for flow processes

Urval Satish Patel [a,*], Andy Gardiner [b], Dorrik Andrew Vincent Stow [b]

[a] Institute of GeoEnergy Engineering, Heriot-Watt University Malaysia, No 1 Jalan Venna P5/2, Precinct 5, 62200 Putrajaya, Malaysia
[b] Institute of GeoEnergy Engineering, Heriot-Watt University, Riccarton Campus, Edinburgh, EH14 4AS, Scotland, UK

ARTICLE INFO

Article history:
Received 22 June 2021
Received in revised form 7 September 2021
Accepted 7 September 2021
Available online 13 September 2021

Editor: Dr. Brian Jones

Keywords:
Turbidites
Debrites
Massive
Grès d'Annot
Confined basin

ABSTRACT

In high-density turbidite (HDT) systems, proximal deposits typically show thick beds of massive and/or stratified sandstone capped by a thin low-density turbidite (LDT) interval of finer-grained laminated and rippled sandstone. Distally, the massive/stratified HDT interval thins and is replaced by the LDT interval as the dominant facies. Whereas this empirical observation is common to many ancient systems worldwide, a very different relationship is found in the topographically confined Peïra Cava sub-basin in SE France. Eight prominaent beds can be correlated across much of the exposed basin (3 x 11 km). Three massive sandstone facies are recognised in these beds: (1) ungraded (2) graded, and (3) massive with patchy texture. In proximal and medial sections, these facies are capped by a relatively thick LDT interval comprising up to 30% of the bed thickness. Moving to distal sections, the massive facies come to dominate the bed, in some cases forming 100% of the bed thickness. Along a downslope transect, three facies tracts are defined that all differ considerably from previously described trends. Facies tract I and II comprises ungraded massive sandstone and massive sandstone with patchy texture in distal sections, respectively. Facies tract III comprises repetitive sequence of ungraded and graded massive sandstones in distal sections. Statistical analysis of the vertical internal character in the eight beds show non-random, non-cyclic facies trends, with each massive facies exhibiting some level of dependency on other facies, suggesting sediment deposition depended on temporally evolving flow conditions. The ungraded and graded massive facies are interpreted as deposits of high-concentration near bed layers beneath surge-type turbidity currents. In contrast, the massive sandstone with patchy texture is interpreted to result from liquefied debris flows. Bed thickness trends and the presence of distinctive grain size breaks indicate depositing flows were bipartite (debris flow with an overlying concentrated turbulent layer), depletive, unsteady and pulsatory in proximal locations, but evolved distally into a turbulent flows with a simple surge structure. The distal dominance of these massive facies is here interpreted as a consequence of flow interaction with confining topography. This interaction induced gravity and body transformations in flows of facies tract I and II, whereas generation and passage of internal waves in distal sections created the necessary conditions for massive sandstone deposition in facies tract III.

1. Introduction

Massive sandstones are ubiquitous in many ancient and modern deep-water systems. They are a classification of deposits defined by a complete lack of primary sedimentary structures (Stow and Johansson, 2000); a characteristic which has often prevented a conclusive interpretation of their transport and depositional mechanism(s). Nonetheless, investigations of the vertical and lateral distribution of massive sandstones in multiple locations have revealed that the depositing sediment gravity flow leaves a predictable internal facies architecture and distribution; in proximal and medial setting, a bed predominantly comprises massive and/or thick to thin stratified sandstone intervals, which is capped by low density turbidites (Tb to Td division; e.g. Hirayama and Nakajima, 1977; Lowe, 1982; Macdonald, 1986; Tokuhashi, 1989; Mutti, 1992; Remacha et al., 2005; Amy and Talling, 2006; Mcintosh, 2007; Talling et al., 2007a; Sumner et al., 2012; Talling et al., 2013; Malgesini et al., 2015; Cunha et al., 2017). Moving along a downslope transect, the massive sandstone interval transitions (gradually or abruptly), and is replaced as the dominant facies by the low density turbidite interval. This trend has been incorporated into the facies tract of Lowe (1982), Mutti (1992) and Kneller and McCaffrey (2003), and has led many sedimentologists to infer a high density turbiditic origin to massive sandstones (Amy et al., 2005; Amy and Talling, 2006; Sumner et al., 2012; Talling et al., 2012).

* Corresponding author.
E-mail address: u.s.patel@hw.ac.uk (U.S. Patel).

https://doi.org/10.1016/j.sedgeo.2021.106001
0037-0738/

However, in structurally- or salt- controlled basins (i.e. confined basins), the depositing flow can and does encounter lateral and downstream basin margins (Amy et al., 2004; Cunha et al., 2017; Tinterri et al., 2017; Tinterri and Piazza, 2019). Depending on the height of the flow and topography, the angle of incidence and slope geometry, a flow encountering these margins can be reflected, deflected or constricted (Patacci et al., 2015). Such interactions can modify the behaviour of the flow and lead to distinct deposit architecture that deviates from the conventional predictive structure observed in other basins (Kneller et al., 1991; Patacci et al., 2015; Tinterri et al., 2017). Both confined basins and massive sandstones are an important exploration target for the hydrocarbon industry. Thus, knowledge of the vertical and lateral distribution of massive sandstones, as well as the bed-scale internal facies architecture in confined basins is vital. Uncertainty in these aspects can have a fundamental impact on exploration and development of hydrocarbons, and lead to reservoir connectivity issues, reduced sweep efficiency, and incorrect production strategies and project economics.

The main objective of this study is to document bed-scale vertical and lateral distribution of massive sandstones in the Peïra Cava sub-basin (part of the larger Grès d'Annot Basin; Fig. 1a) of south-east France. The Peïra Cava sub-basin is a well-known example of a topographically confined basin, analogous to the modern day intraslope basins of the Gulf of Mexico, in which beds can be correlated over a distance of ~11 km (Hilton, 1994; Pickering and Hilton, 1998; Amy, 2000; Cunha et al., 2017). This allows the vertical and lateral description of the deposit architecture. For this study, eight laterally extensive beds are correlated across the sub-basin. The depositional mechanisms of the massive sandstone intervals are then interpreted based on their vertical and lateral distribution. This interpretation takes into account the effects of flow reflection, deflection and/or transformation induced by the basin margins. It is shown here that the distribution of massive sandstones in topographically confined basins deviates from previous empirical evidence based on field studies.

2. Geological setting

2.1. Regional setting

The Eocene-Oligocene Grès d'Annot Formation of SE France and NW Italy forms a widespread lithostratigraphic unit that represents deep-water sedimentation in the deeper parts of the Tertiary Alpine Foreland basin (Fig. 1b). The basin was located west of the developing Alpine thrust belt and north of the emergent Pyrenean-Provençal mountain belt (Ravenne et al., 1987; Pickering and Hilton, 1998; Sinclair, 2000). The Grès d'Annot Formation is the topmost unit in a sequence comprising the Calcaires Nummulitiques (a bioclastic nummulitic limestone) and the Marnes Bleues (hemipelagic marls), which together represent the gradual deepening and migration of the foreland basin (Fig. 1b; Apps, 1987). Deposition of the formation occurred in a series of small, north-south trending, sub-basins that were created by the folding of the underlying Mesozoic strata during the Eocene regional flexure (Apps, 1987). These sub-basins were separated by topographic highs (100's of metres in height), as demonstrated by the common occurrence of onlap relationships between the Grès d'Annot and the underling Marnes Bleues (Apps, 1987). Onlaps locally reach angles of 25° and typically have apparent slopes of 3° (Elliott et al., 1985; Apps, 1987).

Sediments of the Grès d'Annot Formation were sourced from the Corsica-Sardinia and Maurès-Esterel massif, which was originally located to the south of the Alpine foreland basin (Bouma, 1962; Ivaldi, 1974; Sinclair, 1994). They were transported northwards, parallel to the basin's axis, and deposited by a variety of sediment-gravity flows (Amy, 2000). Due to the topographic highs, flows were locally reflected and deflected, which significantly influenced deposit character in the sub-basins (McCaffrey and Kneller, 2001). The focus of this study is the Peïra Cava sub-basin, which today is located 25 km north of Nice, and preserved as a synclinal outlier (Fig. 1a, c).

2.2. Study area

The Peïra Cava outlier preserves ~50 m of the Calcaires Nummulitques, 150–200 m of the Marnes Bleues and ~ 1.2 kms of deep water sandstones and mudstones of the Grès d'Annot (Pickering and Hilton, 1998; Amy, 2000). The latter has been interpreted as deposits of waning turbidity currents, with minor contribution from debris flows and other deep water processes (Bouma, 1962; Stanley et al., 1978; Pickering and Hilton, 1998; Amy, 2000). The initial basin fill is interpreted to be laterally discontinuous, filling in base of slope scours and topographic lows in the basin floor (Amy, 2000; Lee et al., 2004; Aas et al., 2010). However, subsequent sediment gravity flows produced a sheet-like architecture, with individual beds correlatable in the cross-stream direction for ~3 km and downstream for ~11 km (Pickering and Hilton, 1998; Amy, 2000; Amy et al.,

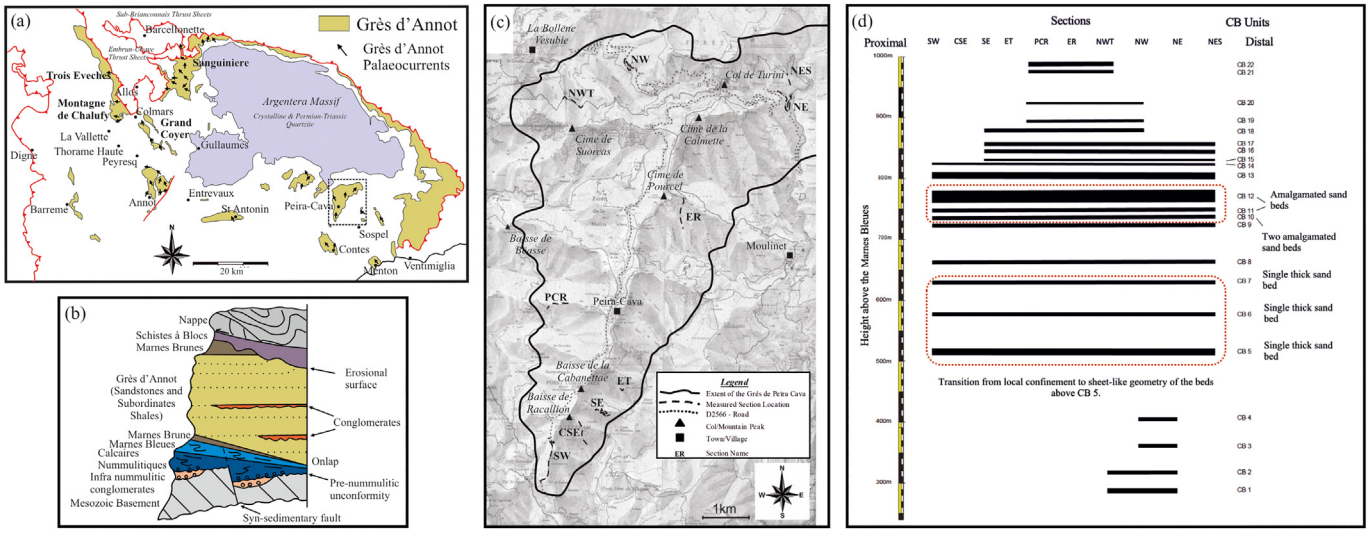

Fig. 1. a) Map showing the geographic distribution of the Grès d'Annot and the location of the Peïra Cava sub-basin in SE France (modified from Apps, 1987). b) Lithostratigraphic column of the sedimentary succession in the Peïra Cava sub-basin recording the progressive deepening of the foreland basin (modified after Ravenne et al., 1987). c) Map of the Peïra Cava sub-basin showing the location of the measured sections of the eight correlatable beds. Section names follow Amy (2000). Base topographic map is the Vallée de la Bévéra 1:25000, 3741 ET, IGN Map. d) Simplified correlation of the major correlatable units in the Peïra Cava. Eight beds are selected to investigate the vertical and lateral distribution of massive sandstone facies. CB 5 to 7 are single sandstone beds, while CB 10 and 11 are amalgamated units consisting of 2 and 3 beds, respectively (modified after Amy, 2000).

2007; Cunha et al., 2017; Patel, 2018). To the south, the Mention and Contes sub-basins are interpreted as canyon feeder systems and the proximal equivalent of the Peïra Cava sedimentary fill (Fig. 1a; Hilton, 1994; Amy, 2000; Joseph and Lomas, 2004). Thus, the present depositional model of the Grès d'Annot in the study area envisions flows travelling northwards through the Contes (and Mention) sub-basin, before travelling sub-parallel to the strike of the western lateral slope of the Peïra Cava sub-basin and depositing their sediment load. The basin is interpreted to be confining in nature and ponding of the flows is based on: i) onlap relationship of the Grès d' Annot and the underlying Marnes Bleues, ii) thick mudstone caps, iii) anomalous orientation of palaeocurrent and erosive structures, indicative of flow reflection and deflection, iv) thick beds positioned adjacent to the base of slope, v) repeated or stepwise normal grading, and iv) grain size sorting across the topography suggesting flow stripping (Sinclair, 1994; Kneller and McCaffrey, 1999; Amy et al., 2004; Cunha et al., 2017).

2.3. Peïra Cava sub-basin configuration

The configuration of the Peïra Cava sub-basin (and the wider Alpine Foreland basin) is inherited from movement along shallow Alpine thrusts in the underlying Cretaceous strata (Apps, 1987; Pochat and Van den Driessche, 2007). It exerted a strong control on spatial variation in sediment-gravity flow properties, which in turn controlled sediment facies distribution, the main focus of this study (Amy, 2000; Amy et al., 2004; Amy et al., 2007; Muzzi Magalhaes and Tinterri, 2010; Tinterri et al., 2016; Cunha et al., 2017). Based on onlap relationships and palaeocurrent data, only the western and southern margins of the Peïra Cava sub-basin are preserved (Fig. 2; Pickering and Hilton, 1998; Amy, 2000; Amy et al., 2004; Cunha et al., 2017). The western basin margin was oriented in an approximately northwest to southeast direction, and rotates clockwise to north-northeast to south-southwest moving northwards (Amy, 2000). In southern areas the dip of this slope was between 4 and 7° towards the east, increasing to ~15° between the Baisse de Beasse and Cime de Claudine (Amy, 2000; Amy et al., 2004). Palaeotopographic reconstructions indicates the southern basin margin is a continuation of a northward dipping (~ 8°) slope preserved in the Contes sub-basin (Hilton, 1994). The eastern side of the margin is not well preserved and no onlap relationship is observed. Nevertheless, the presence of a low angle lateral slope is inferred from highly variable palaeocurrent directions, as well as convoluted lamination, alternation of sedimentary structures (i.e. wavy parallel lamination, ripples, biconvex ripples, and small-scale hummocky-type structures) observed along the inferred eastern margin (Fig. 2; Amy, 2000; Tinterri et al., 2016; Cunha et al., 2017). In the northern parts of the sub-basin, the stratigraphy is folded and overturned, and the bounding slope has not been preserved. However, the occurrence of thick mudstone caps separating sandstone beds indicate the northern slope completely ponded the sediment-gravity flows in the sub-basin (Sinclair and Tomasso, 2002). Thus, the simplest sub-basin configuration assumes a western lateral slope with decreasing slope angles to the east (Amy, 2000).

2.4. Sea-floor bathymetry

Aas et al. (2010) reconstructed the Peïra Cava sub-basin palaeobathymetry through backstripping of overburden and removal of the synclinal structural overprint using surface-based modelling. The modelled sea-floor reveals three bathymetric lows separated by topographic highs (the Rocaillion and Pourcel ridges; Fig. 2), which initially ponded large flows in proximal locations (Amy, 2000; Lee et al., 2004; Aas et al., 2010). However, the degree of confinement lessens as the proximal bathymetric lows were filled, and the flows spilled over to distal part of the sub-basin. The transition from local confinement to sheet-like geometry of the beds occurred just prior to the deposition of a distinct marker bed called 'CB 5' (Amy, 2000; Amy et al., 2007; Aas et al., 2010). The absence of channel elements and infrequent bed amalgamation,

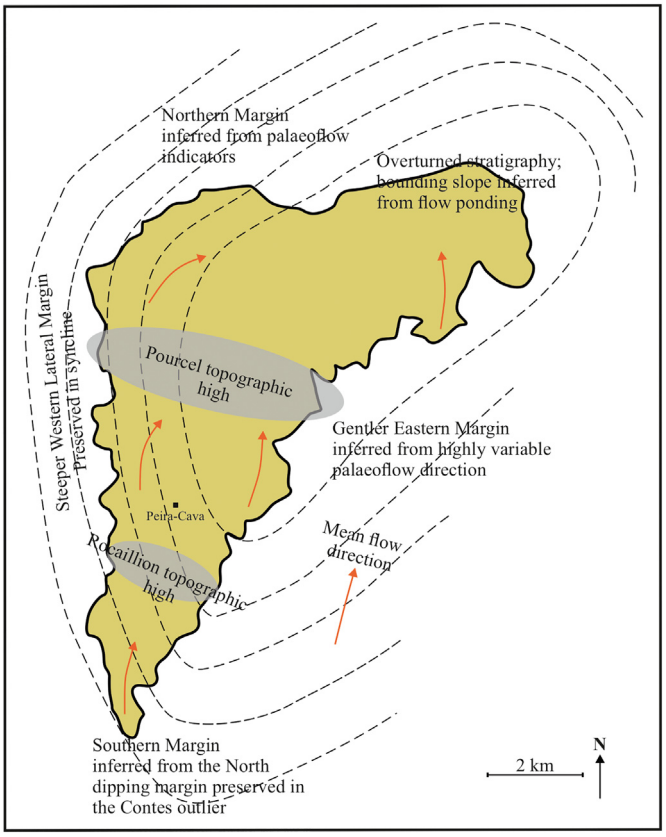

Fig. 2. A schematic diagram showing the basin configuration and palaeotopographic highs within the Peïra Cava sub-basin. Flows travelled northwards and were reflected/deflected by the lateral and bounding slopes. The palaeotopography ponded flows below CB 5 in proximal locations. Above CB 5, correlation of beds across the outlier show proximal confinement lessens and the beds obtaining a sheet-like geometry.

especially in distal locations, further attest to basin-wide deposition above marker CB 5 (Aas et al., 2010). Above CB 5, the seafloor in the sub-basin may have also been locally irregular (metre-scale), as indicated by erosive scours, biconvex ripples, convolute laminations, and depositional relief (Tinterri et al., 2016; Cunha et al., 2017). Proximality trends in bed thickness also indicate sandstone beds thinned distally across the outlier. Despite these controls on bed geometry, the system aggraded uniformly with irregularities on the sea-floor being smoothed out by mud deposition (Amy, 2000). Thus, the Peïra Cava sub-basin sea-floor is assumed to be relatively flat (Aas et al., 2010).

3. Data and methods

3.1. Correlation framework and sedimentary logs

This study focuses on eight laterally correlatable beds in the Peïra Cava outlier (Fig. 1d). These eight beds correspond to CB 5, 6, 7, 10 and 11 of Amy (2000) and Amy et al. (2007). CB 10 and 11 are packages of beds, consisting of two and three beds respectively (Fig. 1d). Individual beds within these packages have the suffix −1, −2, etc. to differentiate them. Fig. 1c shows the location of ten sections in the Peïra Cava outlier were the beds were studied. All the beds were chosen due to the ease with which they can be recognised in the field and the presence of massive (i.e. structureless) intervals along their downslope facies tract. The eight beds were also the most easily accessible and widely exposed in the outlier, especially compared to marker beds below CB 5.

After locating the beds in the field, a detailed sedimentary log was created at a scale of 1:10. Grain size was measured every 2–5 cm using a grain size comparator and at smaller intervals where abrupt changes in grading occur or where grain size breaks were observed. This method

biases the measurement to the coarsest 5 to 10% of the grain size distribution within the sandstone bed, as measured from thin section analysis (see below; Talling et al., 2004). Nevertheless, it allowed the dominant grain size range to be measured in the field and provided a reliable measurement of relative grain-size changes between beds. Palaeocurrent measurements were taken from sole marks. Bed thicknesses were measured with a standard measuring tape orientated perpendicular to the bed. Sedimentary facies were described using a hierarchical descriptive facies scheme that describes the units initially on (i) lithofacies, and then on (ii) subfacies based on sedimentary structures (Table 1). Outsized clasts (sand and mud) and dewatering structures were not incorporated into the facies scheme, but appear as accessory features within each facies. Thus along a facies tract, discrete beds will be composed of lithofacies and subfacies arranged vertically and laterally. The facies scheme is based on the general process-based facies tract by Mutti (1992), later modified by Amy (2000) and Cunha et al. (2017) for use in the topographically confined Peïra Cava sub-basin.

3.2. Textural analysis

Field samples were collected from four beds at regular intervals to confirm the qualitative measurement of grain size in the field, and provide additional information on the textural characteristics, including the vertical grading, sorting and mud content. The samples were selected from CB 5 (NE section), 10-1 (NWT section), 10-2 (NES section) and 11-2 (NES section). Quantitative measurements on the size and sorting of grains (inclusive graphic standard deviation of Folk and Ward (1957)) were generated by image analysis using SEM backscatter electron (BSE) images. A minimum of 300 quartz, feldspar or lithic grains coarser than 8 μm were measured from each BSE image. The mud content was estimated by thresholding the images to isolate the clay component and calculating the percentage area occupied after binarisation of the image.

3.3. Embedded Markov chain and entropy analysis

Embedded Markov chain and entropy analysis was used to analyse the vertical arrangement (against a null hypothesis of independence) and degree of random occurrence of facies within the logged beds, respectively. Both analyses are useful in defining genetically related facies, distinct vertical trends, and interpreting transport and depositional processes. For this study, the procedures follow that of Powers and Easterling (1982) and Hattori (1976), respectively. In both analyses, the transition from one facies to the same facies is not recorded, even in situations where they are observed. In the present study, such a state may arise when the facies is separated by a grain size break. The thickness of the facies is also not considered in either analysis, since it does not influence the formation of massive sandstones, but is considered a product of flow duration and/or flow thickness (Kneller and Branney, 1995). Furthermore, only the sand and coarser facies within the studied beds are subjected to the analysis in order to reduce diffusion of transitions between the sand and mud lithofacies. And lastly, the vertical to lateral transition in facies was not investigated using either analysis due to the inherent complexity of downslope transitions where timelines may not be horizontal.

The output of the Markov Chain analysis is a vertical facies relationship diagram. In this study, the statistically significant transition (limiting value of 0.1 based on the difference matrices) and the observed facies transition (i.e. transition count matrices) are employed to construct the diagrams. The output for the entropy analysis is a set of diagrams showing the distribution of entropy pairs; 1) entropy after the deposition (i.e. post-deposition), which refers to leaving a particular j^{th} state for any other state and is designated as E(Post), and 2) entropy before deposition (i.e. pre-deposition), which refers to entering a particular j^{th} state from any other state E(Pre). The values of E(Post) and E (Pre) are normalised and plotted to show the inter-relationship between the two entropies. These are then compared to models presented by Hattori (1976) to classify various cyclic patterns into asymmetric, symmetric, truncated (lower, upper or both), or random cycles.

For the statistical analysis, the locations of the measured sections are grouped into one of three categories according to their relative position within the sub-basin: proximal (sections SW, CSE, SE, and ET), medial (PCR and ER), and distal (NWT, NW, NE, and NES; Fig. 1c). This approach allows both the statistical analysis of the vertical arrangement of facies, and therefore the temporal evolution of flow processes, and the qualitative characterisation of the downslope facies transition and arrangement.

4. Results

A series of correlation panels of the eight beds, illustrating the vertical and lateral variability in bed geometry and architecture, are presented in Figs. 3 to 6. These correlation panels, as well as individual vertical section of beds, form the basis for evaluating the bed-scale vertical and lateral distribution of massive sandstones, the flow hydrodynamics, and impact of the confining topography on the internal character. The panels are oriented roughly parallel to the palaeoflow direction and cover a distance of ~11 km. A description of the facies is provided in Table 1, while Fig. 3 shows the key to the sedimentary logs.

4.1. Massive sandstones at a single outcrop

Since the focus of this study is on the massive sands, these facies are described in detail below. For description of other facies, refer to Table 1 and Fig. 7.

4.1.1. Sandstone – ungraded, massive (SM1)

Ungraded, massive sandstones (SM1) facies comprise grains covering the entire sand size range (2 mm to 62 μm). The facies is completely devoid of any primary sedimentary and dewatering structures (Fig. 8a, c). Grain size measurements using a comparator in the field show no vertical grading (Fig. 8a). This is confirmed by thin section analysis, which shows no statistically significant changes in the coarsest 5% of the grain size distribution (Table 2). However, complex grading trends are observed in the finer grain size percentiles in thin sections, and may be indicative of one or more different grain settling processes (Table 2). Mud content is low, typically between 2.1 and 7.1% of the total thin section area. Grain sorting is poor to very poor (between 1.1 and 2.82 phi). Mud clasts are rare, but where present, they are unarmoured, up to 10 cm in diameter, clustered floating, and occurring in a thin zone parallel to the bedding plane or at low angle (with isolated high angle clasts; Fig. 8a, b). They are typically elongated, with a-axis approximately parallel to the bedding plane. Grain size trends below and above the mudclast zone are stable. Intervals of SM1 facies are commonly overlain by graded, massive sandstones (SM2) or intervals consisting of thin, spaced stratification (SL2).

4.1.2. Sandstone – graded, massive (SM2)

Similar to the SM1 facies, this facies is devoid of primary sedimentary structures and consists of grain size covering the sand size range (2 mm to 62 μm; e.g. PCR and NWT CB 10–2). Vertical normal grading is observable in the field using a grain size comparator (Fig. 8c), but is only recognisable in the coarsest 5% of the grain size distribution. Grain size measurements from thin sections confirm this trend, but is further characterised by complex grain size trends (i.e. fining or coarsening fine-tail distribution) with increasing height from the base of the facies (NE CB 5; Table 2). Locally, subtle inverse grading is also visible in this facies. Mud content is relatively low (between 2.6 and 4.7%) and grain sorting ranges from moderately (0.8) to very poorly (2.21) sorted. Similar values in the sorting parameter are also observed in other beds based on visual estimates using a grain size comparator. Mud clasts, where present, are granular to medium pebble in size (2

Table 1
Description of lithofacies within the eight studied beds in the Peïra Cava sub-basin.

Facies	Facies Description	Texture			Thickness	Vertical Distribution	Lateral Distribution	Interpretation
		Grading	Grain Size Dist.	Sorting				
SM1 - Ungraded massive sandstone	Massive, ungraded clean sandstone. Mudclasts are dispersed graded to locally clustered floating and ordered stratified.	Ungraded to subtle coarse-tail graded	250 μm-2 mm	Moderate to poor	dm to > m	Base and middle	Proximal to distal, increasing in percentage in distal sections	See text
SM2 - Graded massive sandstone	Massive, graded clean sandstone. Mudclasts typically occur as ordered stratified and dispersed graded.	Normal graded – distribution and coarse-tail grading	187 μm–2 mm	Moderate to poor	dm to > m	Middle and top	Proximal to distal, greater abundance in proximal and medial sections	See text
SM3 - Massive sandstone, 'patchy texture	Massive, ungraded clean sandstone. Patchy texture consisting of irregular 'patches' of coarse grains adjacent to fine grains. Chaotic to locally stratified mudclast conglomerates/breccia.	Ungraded to weakly coarse-tail graded	250 μm-2 mm	Poorly sorted	dm to > m	Whole bed, base and middle	Medial and distal sections	See text
SL1 – Sandstone, laminated	Laminated sandstone, <3 mm thick, planar to wavy, locally convoluted. No grain size variation between laminae. Laminae typically become more distinct upwards in the bed. Laminae traced for metres laterally. Rarely contain <2–3 cm mudclast along distinct horizon.	Normal graded to ungraded	125-354 μm	Moderate to moderately well	cm to > m	Top of beds	Proximal to medial. Rarely distal	Formed from low-density turbidity current in the upper stage plane-bed regime. Experimental work have shown lamination forming via migration and burial of low amplitude bedwaves under low sediment fallout rates.
SL2 – Sandstone, thin (mm to <1 cm) spaced stratification	Alternating coarser and finer grained laminae. 3 - <10 mm thick. Laminae thickness decreases with height from base, and becomes more distinct towards the top. Planar to locally wavy/irregular, sharp contacts. Individual laminae are ungraded to normal and inverse graded. Laminae traced for cm at base, increasing towards the top.	Weakly normal graded	354 μm-1.5 mm	Poor to moderately poor	cm-dm	Middle and top	Proximal and medial sections	Formed by concentrated turbidity currents from near bed high-concentration layers with sediment concentration of 10–40%. Hindered settling and frictional interlocking of grains are likely to play important roles in these layers. The layers are fed and driven by the overriding current. Shearing of the layers and partial erosion by the current produces a crude planar stratification, that become more defined at lower sediment-fallout rates.
SL3 – Sandstone, thick (> 1 cm.) spaced stratification	Thick (>1 cm to <15 cm), alternating coarse and fine grained lamination. Thickness of individual layers decreases with height from base. Diffuse and irregular at the base, become more distinct upwards. Sharp to gradational contacts between lamination. Coarser laminae are typically ungraded, but rarely normal and inverse graded. Finer grained laminae are normal graded.	Normal graded	545 μm-4 mm	Poor	dm to > m	Base and middle	Exclusively proximal	Not reproduced in experimental studies. Thought to be produced by similar processes to above but wth coarser grain sizes, higher sediment concentrations and higher shear stresses. Traction carpets of Hiscott (1994b), Sohn (1997).
SR – Sandstone, rippled	Ripple cross lamination, planar to trough, climbing ripples. Locally convoluted. Wavelength < 15 cm and typically <10 cm.	Normal graded	125-354 μm	Moderate to well sorted	cm-dm	Exclusively top of beds	Predominantly proximal to medial	Unambiguous evidence of deposition from low density turbidity currents. Sand reworked as bedload into ripples in the lower flow regime. Relatively low rates of sediment fall-out.
ZM – Siltstone, massive	Massive, gradational contacts to the underlying sand and overlying mud.	Ungraded, to normal graded	n/a	n/a	mm to dm	Exclusively top of beds	Proximal sections	Sedimentation via settling flocs at the rear of a dilute, fine grained turbidity

(continued on next page)

Table 1 (*continued*)

Facies	Facies Description	Texture			Thickness	Vertical Distribution	Lateral Distribution	Interpretation
		Grading	Grain Size Dist.	Sorting				
	Abundant carbonaceous fragments							current.
ZL – Siltstone, laminated	Planar laminated siltstone, fissile, gradational contact, abundant carbonaceous fragments	Ungraded to normal graded	n/a	n/a	mm to dm	Exclusively top of beds	Rarely in distal section, predominantly in proximal and medial	Not reproduced in experimental studies to satisfactory degree. Thought to be produced by tractional reworking beneath a dilute, fine grained turbidity current.
MM – Mudstone, massive	Massive (massive), minor silt fraction at the base	n/a	n/a	n/a	cm to > m	Mudstone cap at top of beds	Proximal to distal, increasing in thickness and preservation in distal sections	Static settling of clay or formation of fluid mud layers from a collapsing mud cloud
ML – Mudstone, laminated	Laminated mudstone. Laminae are 0.1 to <1 mm thick. Locally the laminae are silt/ v.f grained. Fissile.	n/a	n/a	n/a	cm-dm, rarely >1 m	Mudstone cap at top of beds	Predominantly in proximal locations, decreasing in thickness distally	Settling of flocs from a dilute and expanded suspension cloud. Rapid suspension of mud laminae upon dampened turbulence. Silt laminae are deposited when the mud flocs are broken up by shearing from the flow.
CM1 – Conglomerate, clean, matrix supported/Pebbly sandstone	Matrix-supported conglomerate, mixture of cobble, and pebble material floating in a matrix of poorly sorted coarse sand to granules. Massive. Mud- and sandclasts, where present, are disorganised and chaotic distributed to locally inversely/normally graded and ordered stratified. Mud- and sandclast vary in size from cm to >1 m locally.	Dispersed graded mud and sand clasts. Coarse-tail grading in the matrix component	Matrix – 545 μm-4 mm. Clasts - >4 mm - <3 cm	Matrix – moderately to poorly sorted. Clasts – poorly sorted	dm to >1 m	Base of beds	Predominantly in proximal to medial sections, rarely in distal sections	Non-cohesive debris flows, hyperconcentrated flows or inflated sandflow with ~40–70% concentration by volume, characterised by excess pore pressure and grain to grain interaction upon flow deceleration. Deposition occur via en-masse freezing due to interlocking of grains. High hydraulic diffusivity and well connected pores allows flow transformation to concentrated turbidity currents downslope.
CM2 – Conglomerate, clean, clast-supported	Clast-supported conglomerate, massive (massive), locally stratified. Mud- and sandclasts, where present, occur either along distinct horizon (ordered stratified) towards the top of beds or chaotically distributed towards the base. Mud- and sandclast vary in size from cm to >1 m.	Dispersed graded mud and sandclasts. Coarse-tail grading in the framework component.	Matrix >4 mm. Clasts - > 6 mm - < 16 cm	Moderately to poorly sorted	dm to >1 m	Base of beds	Proximal and medial locations	Non-cohesive debris flows, hyperconcentrated flows or inflated sandflow with ~40–70% concentration by volume, characterised by excess pore pressure and grain to grain interaction upon flow deceleration. Deposition occur via en-masse freezing due to interlocking of grains. High hydraulic diffusivity and well connected pores allows flow transformation to concentrated turbidity currents downslope.
CM3 – Conglomerate, mud-rich, matrix-supported	Chaotic/disorganised unit consisting of floating clasts in a muddy matrix. Mud- and sandclasts are disorganised and consist of marls, limestones and turbidite beds. Clasts range in size from cm to >1 m.	Disorganised	Matrix – mud. Clasts – cm to >1 m	Very poorly sorted	dm to >1 m	Base of bed	Exclusively in proximal sections	Highly to moderately cohesive debris flow characterised by matrix strength which provides the main grain support mechanism for clasts. Liquefaction and grain interaction may be locally important. Moderate to high clay content imparts low hydraulic diffusivity. The flow comes to rest en-masse.

mm – 16 mm) and rarely greater than 5 cm. They are predominantly ordered stratified; aligned along the long axis and occurring within thin zones parallel or at a low angle to the bedding plane (e.g. SE CB 10-2 Fig. 8d). The larger clasts are isolated and tend to be more tabular with increasing clast size. Secondary dewatering features are present only in one location (PCR CB10-2; Fig. 8f) where they occur as widely-spaced consolidation laminae, passing into shallow dish structures and pipes towards the top. Intervals of SM2 facies are commonly overlain by structured intervals consisting of SL2 and parallel lamination (SL1) facies.

4.1.3. Sandstone – massive, patchy texture (SM3)

Massive sandstone with patchy texture (SM3) are relatively rare and consists of juxtaposed irregular patches of poorly sorted coarser and

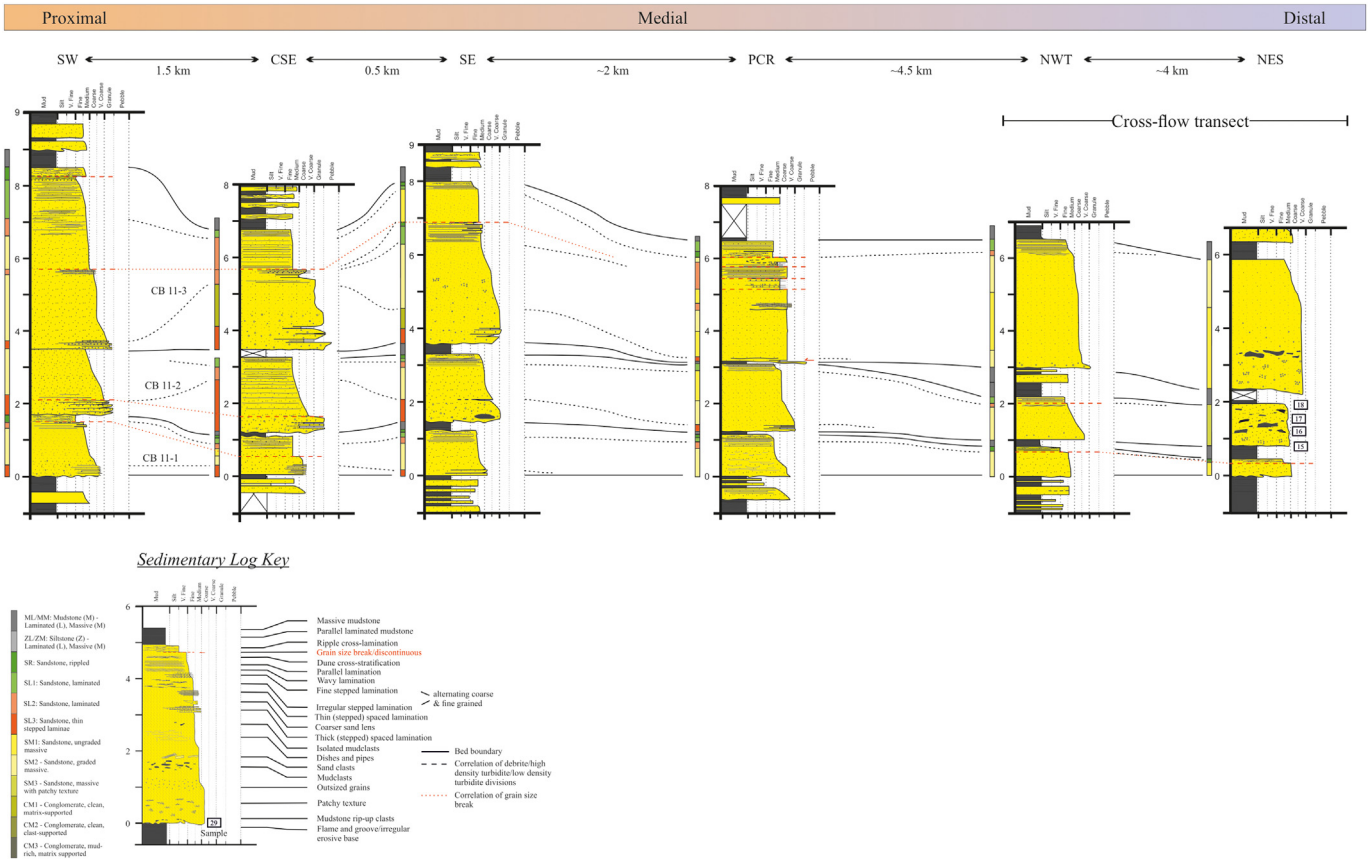

Fig. 3. Correlation panel of CB 11 beds showing lateral changes in internal bed character and external geometry. The panel is oriented roughly parallel to the palaeoflow direction. Solid black lines represent bed boundaries, dotted black lines represent transition between debrite, high-density turbidite and low-density turbidite deposits, and dashed red lines represent correlation of grain size breaks between sections. The key to the sedimentary logs is also provided. (For interpretation of the references to colour in this figure legend, the reader is referred to the web version of this article.)

better sorted finer material (Fig. 8e). The facies is equivalent to the swirly or patchy texture massive sandstone facies (Cs7) of Talling et al. (2012) and Talling et al. (2013). Grain size ranges from medium to coarse as measured in the field, which is confirmed in the coarsest 5% of the grain size distribution measured from thin sections (Table 2). Grading is highly erratic due to the juxtaposed coarse and finer grained sediments, which also makes it difficult to observe in thin sections. However, the top 5 to 10 cm of this facies in beds

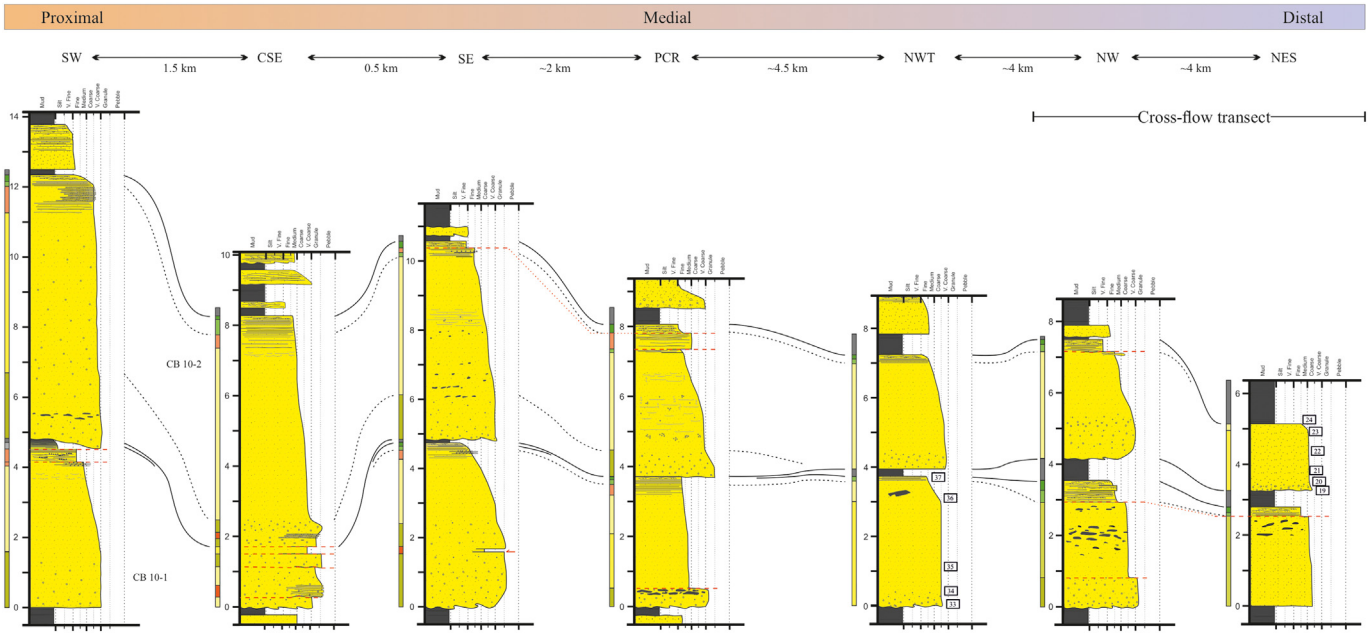

Fig. 4. Correlation panel of CB 10 beds. See Fig. 3 for sedimentary log key and caption for detail.

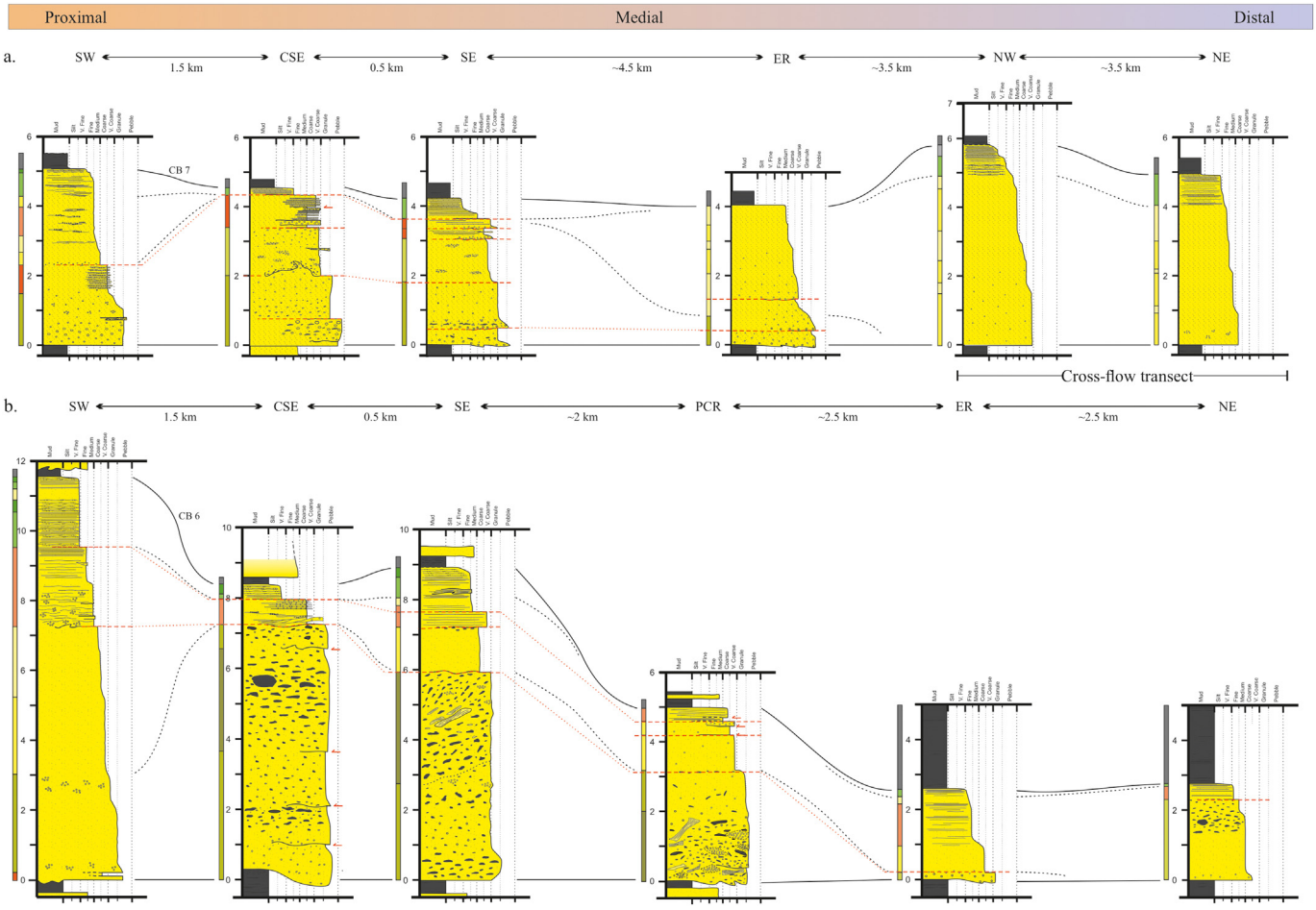

Fig. 5. Correlation panel of CB 7 and 6. See Fig. 3 for sedimentary log key and caption for detail.

commonly shows distribution grading. Sorting is highly variable, ranging from poorly to very poorly sorted, due to the patchy texture. The mud content is low (between 8.3 and 10.3%), but higher compared to the two other massive facies (Table 2). Mudclasts are common in this facies; observable in the middle or towards the top of beds, surrounded by clean sandstone matrix. The clasts vary from small pebble (4 mm) to cobbles (<40 cm) in size and occur as nested discontinuous zones sub-parallel to bedding. They are unamoured, elongated, sub-angular to rounded and are very poorly sorted. In distal locations (e.g. NES, NE), they are generally dispersed graded and less chaotic than proximal and medial locations. Similar to the ungraded and graded massive facies, and based on their composition, the clasts were derived from within the basin. No dewatering (e.g. dishes, pipes and convoluted consolidation laminae) or burrowing features were observed in this facies. The facies typically constitute the basal and middle portion of beds and is separated by a grain size break (i.e. abrupt change in grain size) from overlying facies (i.e. intervals of parallel lamination or thin, spaced stratification; Fig. 5 CB 6).

4.2. Markov chain

Markov chain transition diagrams for the three grouped locations (proximal, medial, and distal) are shown in Figs. 9. The chi-squared statistics for the proximal ($x^2 = 184$) and distal ($x^2 = 52$) location (limiting value of 91 and 42, respectively) indicate a non-random sequence at the 99.5% confidence level. In contrast, the chi-squared statistics for the medial sections ($x^2 = 34.54$ compared to a limiting value of 56.9) indicate that deposition was not by Markovian process. However, at the 97.5% confidence level, the medial sections do reject the null hypothesis. Supplementary data 1 presents the Markov Chain transition count, upward transition, upward expected and the difference matrices.

4.2.1. Proximal Markov Chain

The chi-squared statistic for the proximal sections indicates the hypothesis of quasi-independence can be rejected at the 99.5% confidence level. Based on this, three broad vertical facies trends can be discerned in the proximal locations from the statistical analysis and the observed facies transition (Fig. 9a). Two of the trends begin with either clean, clast-supported (CM2) or mud-rich, matrix supported (CM3) conglomerates transitioning to clean, matrix supported conglomerate (CM1; probability $P = 0.93$ and 0.43, respectively). The CM1 facies is in turn overlain by either SM2 ($P = 0.16$) or SM1 ($P = 0.13$) intervals. Following the SM2 facies path, the first trend follows a transition through an interval SL2 ($P = 0.30$), followed by SL1 ($P = 0.39$) and SR ($P = 0.69$) facies. The SR facies is in turn overlain by finer grained facies (i.e. mudstones). The second trend follows a path through the SM1 facies, transitioning to SM2 facies ($P = 0.23$), which is in turn overlain by SL2 ($P = 0.30$), SL1 ($P = 0.39$) and eventually SR ($P = 0.69$) facies. On a few occasions, the SM1 facies transitions directly to the SL1 facies ($P = 0.16$). The third trend has a thick stratified sandstone (SL3) interval at the base of beds, transitioning to CM1 ($P = 0.30$) or SM2 ($P = 0.16$) facies, and then into SL2 ($P = 0.24$), SL1 ($P = 0.37$) and finally into SR ($P = 0.69$) facies. In each of these trends, the massive sandstones forms the core of the bed.

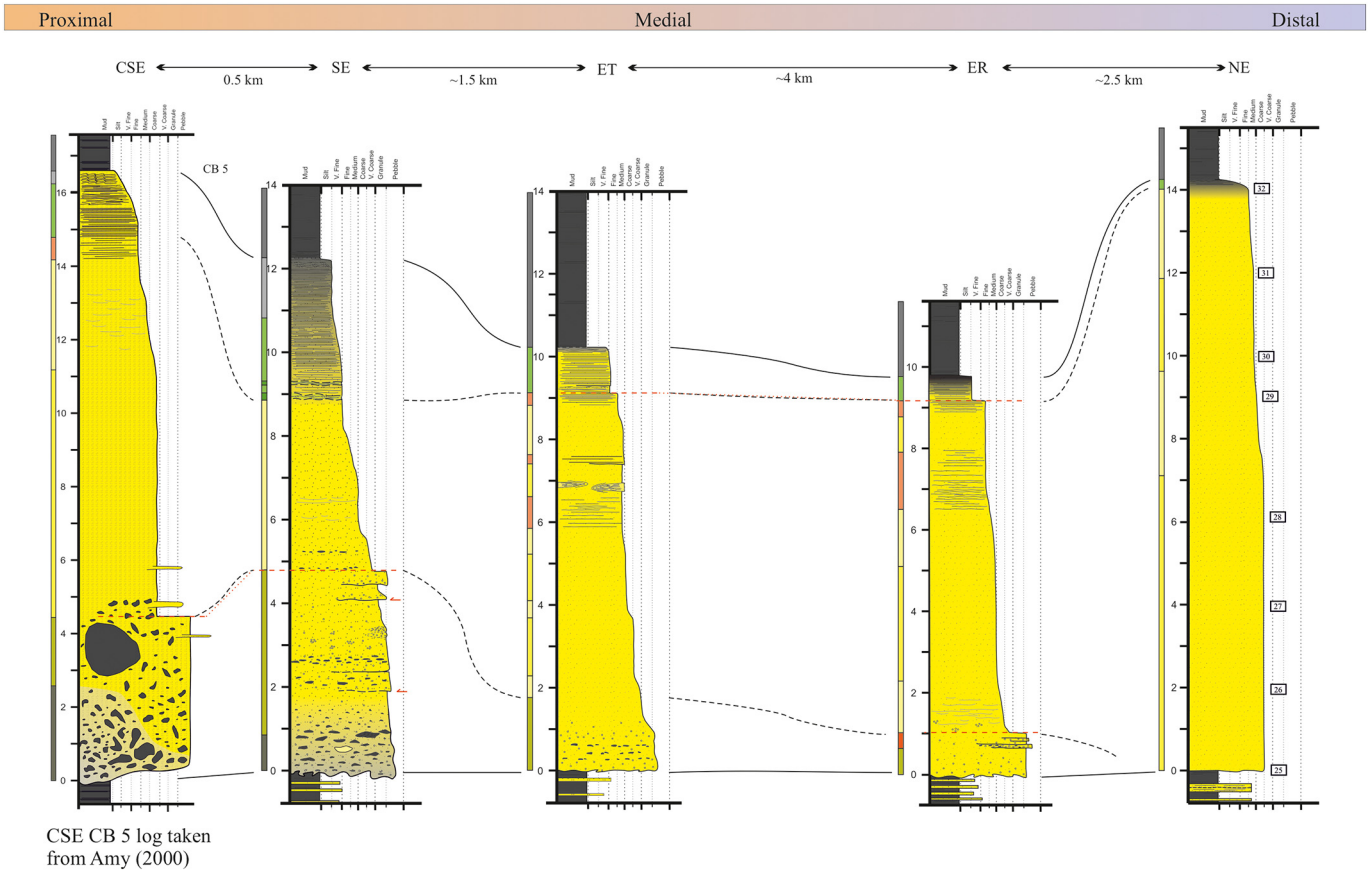

Fig. 6. Correlation panel of CB 5. Sedimentary log at CSE section is taken from Amy (2000) due to the difficulty in accessing the bed in the field. See Fig. 3 for sedimentary log key and caption for detail.

4.2.2. Medial Markov chain

The chi-squared statistic for the medial sections indicate the hypothesis of quasi-independence can only be rejected at the 97.5% confidence level. However, based on observed facies transitions, a general trend (Fig. 9b) can be constructed that includes coarser grain CM1 facies at the base, followed upwards by massive sandstone (either SM1 or SM2), passing into intervals of stratified sandstone (SL1 and SL2) and rippled laminated (SR) facies, and finally terminating with finer grained facies (Fig. 9b). A crude cyclicity that involved repetitive transitions between intervals of SM1, SM2, and SL2/SL1 facies is also discerned from the transition count matrix. Furthermore, locally thick spaced stratification or clast-support conglomerates occur at the base of beds in the medial sections or overly the CM1 facies (Fig. 9b).

4.2.3. Distal Markov Chain

Similar to the proximal location, the chi-squared statistics reject the hypothesis of quasi-independence at the 99.5% confidence level. Based on the statistical analysis and the observed facies transition, two broad vertical facies trends can be discerned (Fig. 9c). The first trend starts with SM1 and SM2 facies at the base. These two facies occur as repeating cycles ($P = 0.13$ and 0.43, respectively), and are eventually overlain by finer grained facies (Fig. 9c). However, the observed transitions also show SL2 and SL1 facies commonly following the massive facies, prior to the transition to finer grained facies. These transitions are not clearly seen from the statistical analysis, but have been incorporated into the Markov chain transition diagrams (dashed lines in Fig. 9c). The second trend shows the massive sand with patchy texture (SM3) preferentially overlain by SL1 ($P = 0.43$) facies, which passes vertically into SR ($P = 0.89$) facies. However, the SM3 facies also has a relative high probability of passing into the SL2 ($P = 0.27$) facies prior to the transition to SL1 ($P = 0.81$). In an isolated case, the SM3 facies is underlain by CM1 facies.

4.3. Entropy analysis

The computed entropy E(Post) and E(Pre), and the respective normalised entropy R(Post) and R(Pre) for each state are shown in Table 3. The analysis shows that the influence of each facies on the preceding or succeeding facies is non-random, but also non-cyclic i.e. asymmetrical trend (Hattori, 1976). For most of the facies in the three geographic locations, the entropies are subequal and $E(Pre) = E(Post) \neq 0$. This indicates a level of dependency of one facies on the other. For a minority of facies $E(Post) = 0$, indicating facies *i* is always succeeded by facies *j* in the sequence (Table 3). Furthermore, the majority of facies states have higher values of E(Pre) compared to E(Post), indicating that succeeding facies states can be discerned with more confidence than those preceding them i.e. these facies exert a strong influence on the succeeding facies state, whilst being less influenced by their predecessor.

4.3.1. Proximal entropy analysis

For facies SL1, SL2, SM2, SM3 and CM3, $E(Pre) > E(Post)$, which indicate deposition of these facies did not depend on precursor facies, but had a strong influence on their successor. Facies SM3 and CM3 have $E(Post) = 0$, implying these facies are succeeded by specific facies (SL3 and CM1, respectively) in the sequence. For the remaining facies, SR, SL3, SM1, CM1 and CM2, $E(Post) > E(Pre)$, indicating that they were deposited under specific depositional conditions, with each facies strongly dependent on the preceding facies. This is more so for the SR facies, where there is a large difference between E(Post) and E(Pre). The normalised entropy sets (Fig. 10a) for each state show that facies SR, SL2,

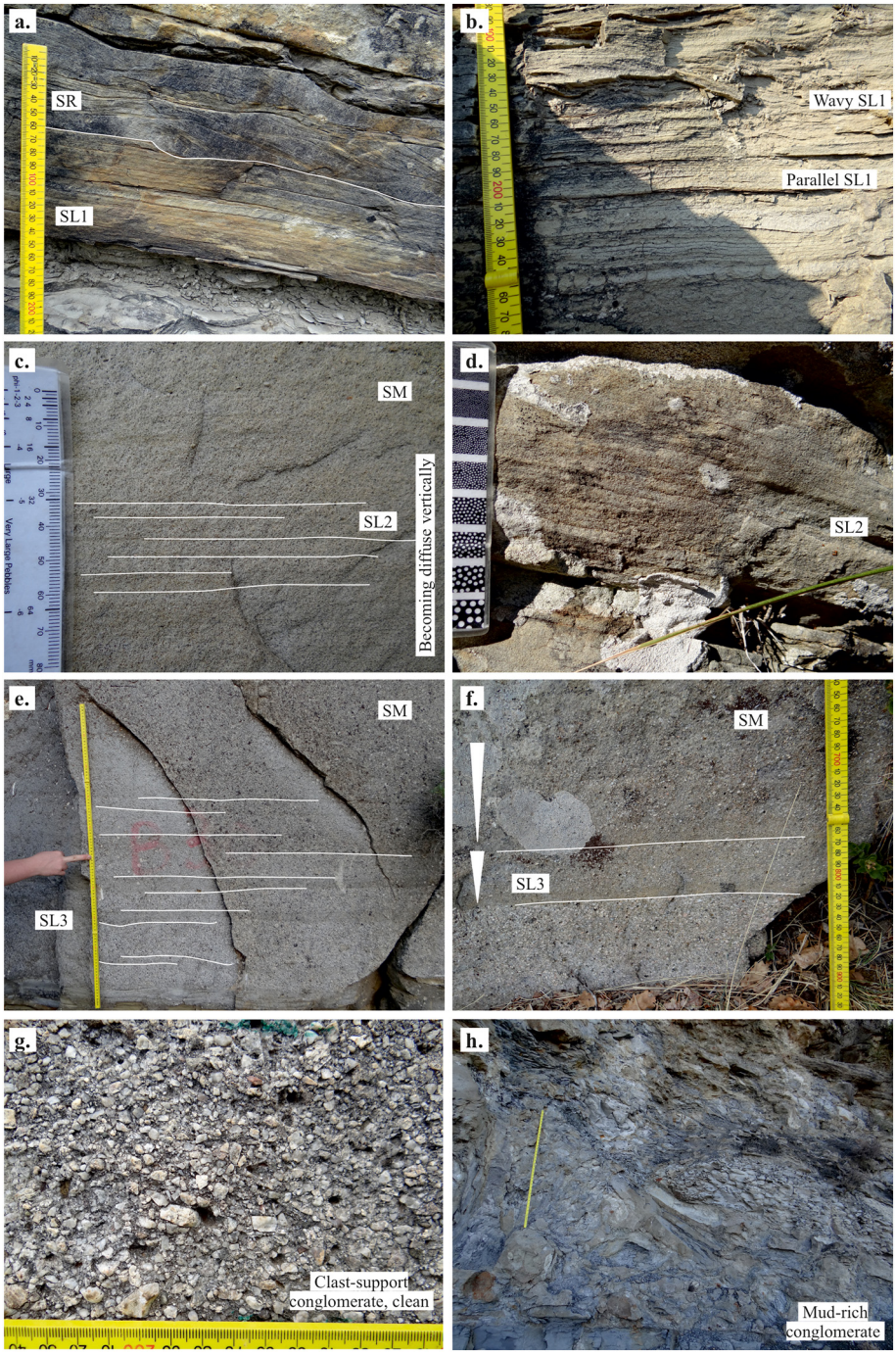

Fig. 7. Outcrop photographs illustrating lithofacies defined in Table 1. a) SL1 facies transitioning to SR at the top. b) parallel to locally wavy SL1 facies. c) and d) SL2 facies; laminae become thinner and more diffuse towards the middle of the image, before transitioning to massive sandstone facies. e) SL3 facies showing < 5 cm to >1 cm thick stratification with step-like normal or inverse grading pattern. g) clean, clast-supported conglomerate. h) mud-rich conglomerate with chaotically organised >1 m long sand- and mud-clasts. The yellow scale is a 1 m ruler. (For interpretation of the references to colour in this figure legend, the reader is referred to the web version of this article.)

SL3, SM1 and SM2, CM1, and CM2 fall within the distribution for A-4 asymmetrical cycle of Hattori (1976). Facies SL1, SM3, and CM3 fall outside this field and may represent lower truncated cycles (Hattori, 1976).

4.3.2. Medial entropy analysis

For facies SR, SL1, SL3, SM2, and CM2, E(Pre) > E(Post), while for SL2, SM1 and CM1, E(Post) > E(Pre). Facies SR and CM2 have E(Post) = 0, and are succeeded by SL1 and CM1, respectively. However, it should be noted that these latter transition occur only once and may not be representative of true cycles or trends. R(Pre) and R (Post) values of the medial facies sets are shown in Fig. 10b. The entropy analysis indicate that the overall facies trends are symmetrical (Hattori, 1976). Facies SL1 and CM2 deviate from this trend, with SL1 having a greater influence on succeeding facies and CM2 on the preceding facies. Despite these results, any interpretation of the entropy sets should be mindful of the fact that medial sections did not meet the chi-squared test for Markovian property. This is most clearly demonstrated for SL2 and SM2 facies, where the large E(Post) and E(Pre) values suggest a variety of facies states can precede or succeed them (Table 3).

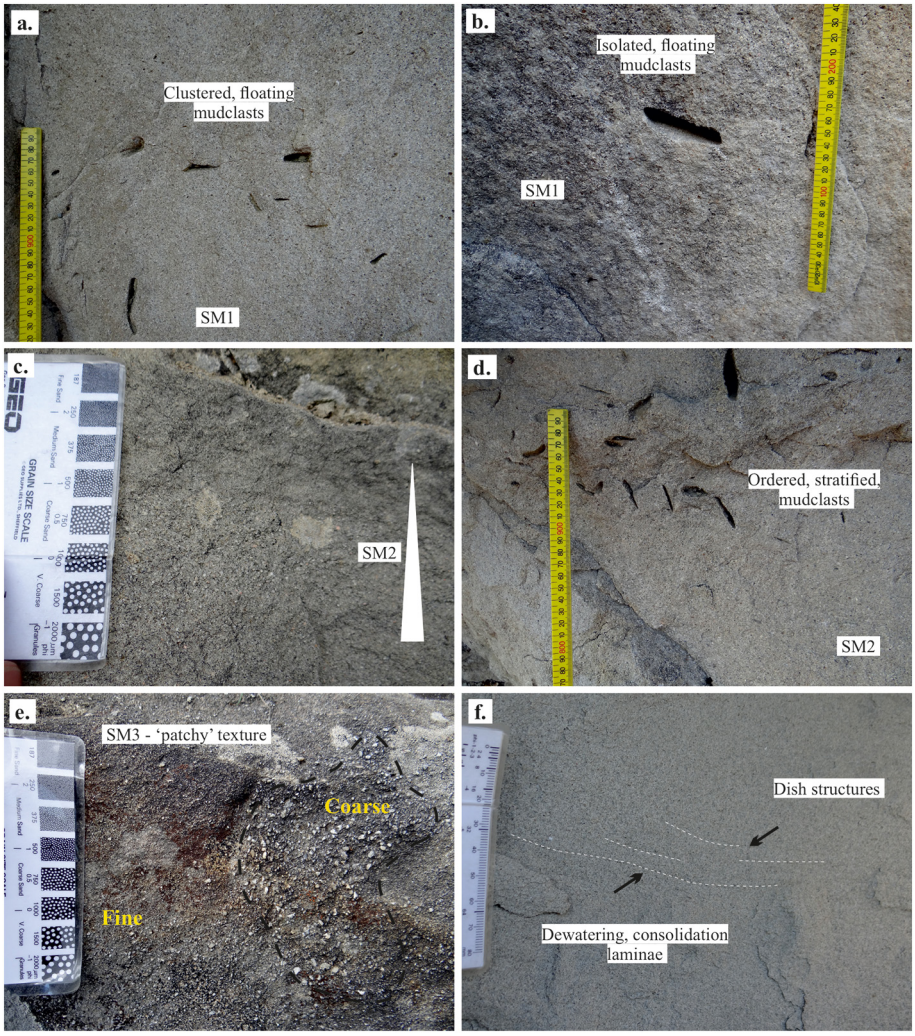

Fig. 8. Outcrop photographs illustrating the massive sandstone facies. a) and b) SM1 facies with isolated or clustered floating <10 cm mud-clasts. c) and d) SM2 facies with or without ordered stratified mud-clasts. e) massive sandstone with patchy texture (juxtaposed patches of coarser and finer grains). f) Dewatering consolidation laminae and dish structures in SM2 facies.

4.3.3. Distal entropy analysis

In distal sections E(Pre) values are higher than E(Post) for facies SL1, SL2 and SM1, indicating they exert a strong influence on the succeeding facies. Facies SM2 and SM3 have entropy sets of E(Post) > E(Pre) and are strongly dependent on the preceding facies state. E (Post) = E(Pre) = 0 for facies SR and CM1, implying preceding and succeeding states for these facies are predicted precisely. However, since facies SR and CM1 form the top and base of beds in distal sections, the entropy sets of these two facies can best be described as truncated upper and lower, respectively (Hattori, 1976). The R (Pre) and R(Post) values are shown in Fig. 10c. Similar to the medial sections, the entropy sets indicate symmetrical facies arrangement. However, normalised entropy values for SL1 and SL2 are more indicative of lower truncated cycles. These truncations are clearly seen in the correlation panels (Figs. 3-6), and are marked by grain size breaks (see below).

4.4. Grain size breaks

The grain size distribution in the eight bed ranges from medium pebble to mud. However, within all examined beds, four types of grain size breaks (i.e. abrupt changes in grain size vertically within a single bed) have been discerned (Fig. 11). Table 4 summaries the characteristics of the observed grain size breaks. The grain size breaks are used to aid interpretation of flow processes, and formation and distribution of massive sandstones.

4.4.1. Type I grain size breaks

Type I grain size breaks separate gravelly and pebbly intervals (16 mm to 2.5 mm) from overlying finer material (4 mm to 500 μm; Fig. 11a, b). This grain size break is only found and correlated at the base and middle of beds in proximal and medial sections (Table 4). In these locations, Type I grain size breaks separate graded and ungraded CM facies from overlying SM1 and SM2 facies in CB 6, 7 and 10–1. The only exception to this trend is seen in CB 11–2 and 5, where SL3 facies is observed below the grain size break, and SL3 and SM facies above, respectively. In CB 6 and 7, the grain size breaks can be correlated to adjacent downslope sections for a distance of ~2–3 km. In both instances, the underlying facies is CM1, while the overlying facies in CB 6 transition from SL2 to SM1. In CB 7, the overlying facies is SM3, which is correlated between sections.

4.4.2. Type II grain size breaks

Type II grain size breaks separate coarser sand (2 mm to 177 μm) from overlying finer grained (1 mm to 62 μm) sediments (Fig. 11c, d). These are observed in a majority of beds from proximal to distal locations. However, in CB 5, 7 and 11–3, they are only observed in proximal

Table 2
Comparison of grain size from SM1, SM2 and SM3 facies as measured in the field and SEM analysis. D10, D50, D90 and D95 correspond to the different percentiles of the grain size distribution. Var, Stand. Dev., Std. Error, and Std. Error Std. Dev. refer to the variance, standard deviation, standard error of the mean, and standard error of the standard deviation respectively. N is the number of grains measured.

Bed/sample	Field measured grain size (μm)	Facies	SEM image analysis (μm/phi)						Summary statistics					
			Mud %	D10	D50	D90	D95	Sorting	Var	Stand. dev	Std. error	Mean	Std. error Std dev.	N
NES CB 10-2/ 24	300–400	SM2	3.4	9.9/6.66	133.3/2.91	325.6/1.62	399.8/1.32	1.9	3.55	1.88	0.02	3.59	0.03	5501
NES CB 10-2/ 23	375–500	SM1	4.5	12/6.37	142/2.82	376.5/1.41	476.9/1.07	1.89	3.01	1.73	0.02	3.25	0.03	5520
NES CB 10-2/ 22	375–500	SM1	7.1	13/6.26	138.4/2.85	351.9/1.51	454.9/1.14	1.6	2.63	1.62	0.02	3.19	0.03	4796
NES CB 102/ 21	375–500	SM1	3.3	11.07/6.50	147.4/2.76	356/1.49	455.2/1.17	1.86	3.09	1.75	0.02	3.27	0.03	4936
NES CB 10-2/ 20	375–710	SM1	6.1	14.5/6.10	149.8/2.74	356/1.49	427.6/1.23	1.73	2.67	1.63	0.02	3.21	0.03	5818
NES CB 10-2/ 19	500–750	SM1	4.5	58.8/4.09	150.4/2.73	381.0/1.39	487.8/1.04	1.24	1.61	1.27	0.01	2.82	0.02	9687
NWT CB10-1/ 37	177–250	SL1	3.1	27.63/5.18	105.1/3.23	190.1/2.39	218.5/2.19	1.06	1.32	1.15	0.01	3.5	0.02	15,805
NWT CB10-1/ 36	375–500	SM2	4.1	61.8/4.02	166.5/2.59	332.6/1.59	407.7/1.29	1.14	1.44	1.2	0.01	2.77	0.03	5646
NWT CB10-1/ 35	710–1000	SM1	2.6	12/6.38	224.5/2.15	554.6/0.85	727.5/0.46	1.93	3.42	1.84	0.03	2.63	0.03	3408
NWT CB10-1/ 34	710–1000	SM1	3.2	12.2/6.35	171.2/2.55	514/0.96	717/0.48	2.08	3.71	1.92	0.02	3.06	0.03	4452
NWT CB10-1/ 33	710–1000	SM1	2.1	12.8/6.34	145.3/2.78	514/0.96	737.2/0.44	2.13	3.78	1.94	0.02	3.21	0.03	5732
NE CB 5/ 32	250–375	SM2	3.4	58.8/4.09	130.1/2.94	230.3/2.12	267.5/1.90	0.8	0.95	0.97	0.01	3.1	0.02	9388
NE CB 5/ 31	250–375	SM2	2.6	12.7/6.30	135.8/2.88	302.7/1.72	376.4/1.41	1.39	2.25	1.5	0.02	3.26	0.04	4314
NE CB 5/ 30	375–500	SM2	3.4	10.2/6.6	142/2.82	387.4/1.37	470/1.09	2.04	3.78	1.94	0.02	3.46	0.04	4303
NE CB 5/ 29	500–750	SM2	4.7	22.6/5.47	213/2.23	502.7/0.99	732.6/0.45	1.49	2.56	1.6	0.02	2.44	0.03	3460
NE CB 5/ 28	710–1000	SM1	4.5	9.8/6.67	202.5/2.30	535.1/0.90	733.7/0.45	2.03	2.56	1.6	0.03	2.47	0.03	2838
NE CB 5/ 27	710–1000	SM1	2.5	11/6.50	168.8/2.57	545.8/0.87	749.7/0.42	2.21	4.47	2.11	0.03	3.17	0.04	3156
NE CB 5/ 26	710–1000	SM1	3.4	11.7/6.61	141.2/2.82	544.9/0.88	737.8/0.44	2.16	4.55	2.12	0.03	3.42	0.04	4137
NE CB 5/ 25	710–1000	SM1	2.3	68.2/3.87	156.7/2.67	500.5/1	705.6/0.5	1.11	1.21	1.1	0.01	2.54	0.03	4011
NES CB11-2/18	177–250	SM3	9.7	26.7/5.25	75.1/3.73	178/2.49	233/2.16	1.03	1.06	1.03	0.02	3.81	0.05	3313
NES CB11-2/17	250–375	SM3	10.3	55.0/4.18	141.8/2.86	345.0/1.54	465.5/1.10	1.76	1.47	1.21	0.02	3	0.03	6069
NES CB11-2/16	300–375	SM3	8.3	10.7/6.54	111.5/3.16	375.3/1.41	587.5/0.77	1.86	3.05	1.74	0.02	3.66	0.04	5371
NES CB11-2/15	250–375	SM3	9.5	19.3/5.61	81.8/3.61	302.9/1.72	522.4/0.94	2.05	1.83	1.35	0.01	3.74	0.03	9538

to medial sections. These three beds all belong to facies tract III (see Section 4.5.3). Across the outlier, Type II grain size breaks are typically located in the middle and top of beds. Grain size breaks located towards the top of beds occur throughout the outlier, while those located in the middle are primarily restricted to proximal and medial sections. In the latter sections, the grain size break located in the middle of the beds predominantly separate SM1 and SM2 facies from overlying SL2 and SL1 facies. This grain size break character has previously been described in

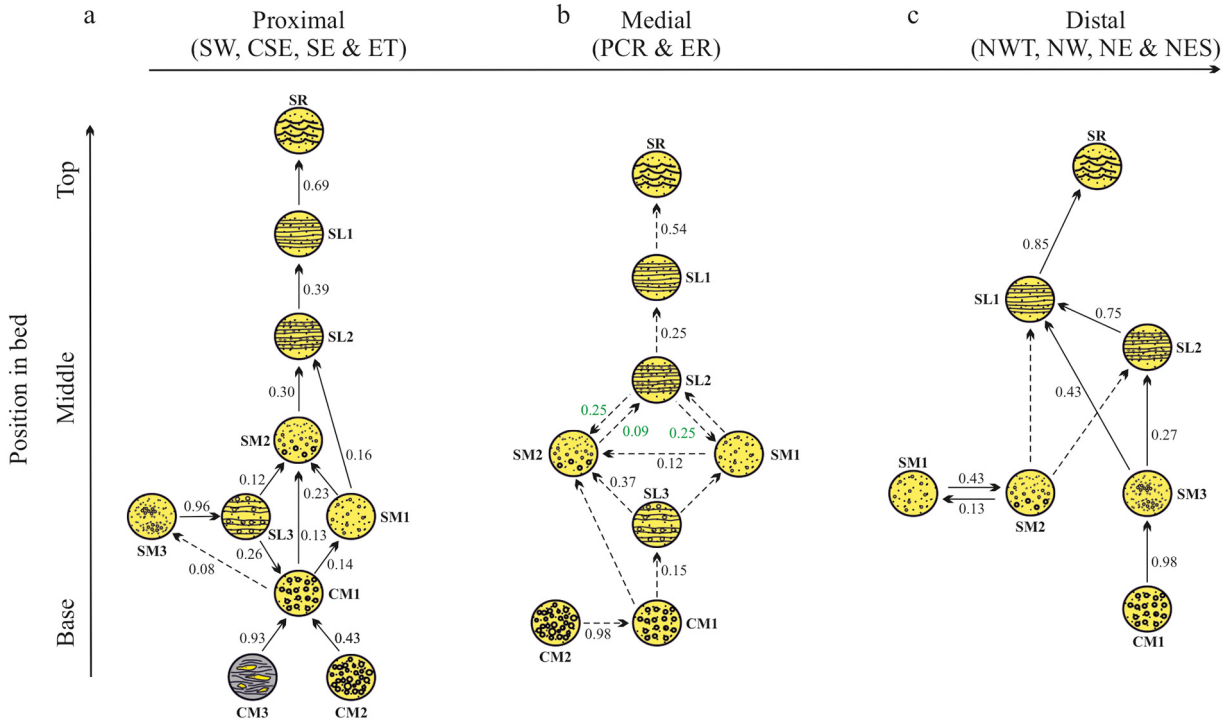

Fig. 9. Markov chain diagrams showing the probabilities of preferred upward transitions for the three section groupings. Solid lines with associated probabilities are based on the difference matrix (minimum probabilities of 0.10 were used for the transitions), while dashed lines are based on observed facies transitions from the transition count matrix. a) Proximal grouping comprises SW, CSE SE and ET sections. b) Medial grouping comprises PCR and ER sections. Values in green are taken from the upward transition probability matrix since the chi-squared value for the medial grouping was below the limiting value at 95% confidence level. c) Distal grouping comprises NWT, NW, NE and NES sections. (For interpretation of the references to colour in this figure legend, the reader is referred to the web version of this article.)

Table 3
Entropy sets for the three section grouping. E(Pre) is entropy before deposition, while E (Post) is entropy after deposition. Together they serve as an indication of the variety of lithological transitions immediately after and before the occurrence of state i, respectively. Where E(Post) > E(Pre), the dependency of state i on the preceeding state is stronger than the influence of state i on the succeeding state. Where E(Pre) > E(Post), state i can follow different state, and is also succeeded by them.

i,j	E(Post)	E(Pre)	R(Post)	R(Pre)	Relationship
Proximal					
SR	1.50	0.71	0.47	0.22	E(Post) > E(Pre)
SL1	0.57	0.59	0.18	0.19	E(Pre) > E(Post)
SL2	1.48	1.61	0.47	0.51	E(Pre) > E(Post)
SL3	2.09	1.82	0.66	0.57	E(Post) > E(Pre)
SM1	1.49	1.23	0.47	0.39	E(Post) > E(Pre)
SM2	1.83	2.13	0.58	0.67	E(Pre) > E(Post)
SM3	0.00	0.53	0.00	0.17	E(Pre) > E(Post)
CM1	2.36	1.89	0.74	0.60	E(Post) > E(Pre)
CM2	1.00	0.67	0.32	0.21	E(Pre) > E(Post)
CM3	0.00	0.50	0.00	0.16	E(Pre) > E(Post)
Medial					
SR	0.00	0.99	0.00	0.35	E(Pre) > E(Post)
SL1	0.92	1.52	0.33	0.54	E(Pre) > E(Post)
SL2	1.91	1.87	0.68	0.67	E(Pre) > E(Post)
SL3	0.39	0.52	0.14	0.19	E(Pre) > E(Post)
SM1	1.03	0.79	0.37	0.28	E(Post) > E(Pre)
SM2	1.82	1.78	0.65	0.63	E(Pre) > E(Post)
CM1	1.46	1.04	0.52	0.37	E(Post) > E(Pre)
CM2	0.00	0.52	0.00	0.18	E(Pre) > E(Post)
Distal					
SR	0.00	0.00	0.00	0.00	E(Pre) > E(Post)
SL1	0.00	0.39	0.00	0.15	E(Pre) > E(Post)
SL2	0.00	0.51	0.00	0.20	E(Pre) > E(Post)
SM1	0.41	0.43	0.16	0.17	E(Pre) > E(Post)
SM2	1.71	1.35	0.66	0.52	E(Post) > E(Pre)
SM3	0.92	0.76	0.36	0.29	E(Post) > E(Pre)
CM1	0.00	0.00	0.00	0.00	E(Post) > E(Pre)

detail by Cunha et al. (2017) in proximal settings. However, in beds CB 7 and 11-3, the opposite facies sequence is observed below and above the grain size break. In contrast, the grain size break at the top typically separate SL3 and SL2 facies from overlying SL1 and SR facies (Figs. 3 and 5). In proximal sections, the grain size break can be correlated between sections, becoming more infrequent and discontinuous in medial sections. Moving distally, there is a gradual change in facies above and below the grain size break, with massive sandstone (SM1 and SM3) below and stratified sandstone (SL1 and SL2) above (e.g. CB 6, 10-1, 10-2, 11-1 and 11-2; Figs. 3-5). Type II grain size breaks in distal sections can be correlated in a downflow and cross-flow direction.

4.4.3. Type III grain size breaks

Type III grain size breaks separate finer gravel and sand (6 mm to 125 μm) from overlying coarser material (16 mm to 375 μm; Fig. 11e, f, g). This grain size break is restricted to proximal (SW, CSE and SE) and medial (PCR and ER) sections, and is observed in all beds except CB11–1 and 11–2. In many of these beds, the grain size break is discontinuous at the outcrop scale, disappearing over a distance of 20 m. Vertically, the grain size break can be observed at any height within the bed. In proximal and medial locations, grain size breaks located at the base of beds separate CM1 facies from an overlying coarser grained CM1 facies. The only exception to this trend is at the base of CB 10–1, where the overlying facies is SL3.

Moving vertically up from the base, Type III grain size breaks are observed in the middle of CB 6 and CB 7 (Fig. 5). In CB 6, the grain size break is observed in the CSE section only, where it separates CM1 facies. In contrast, within CB 7 the grain size break separates CM3 and SL3 facies from an overlying interval of SL3. Moving downslope in CB 7 to the ER section (~4 km), the facies transition to graded massive sandstone above and below the grain size break. Type III grain size breaks located at the top of beds are observed in CB 6, CB 10-2 and CB 11-3

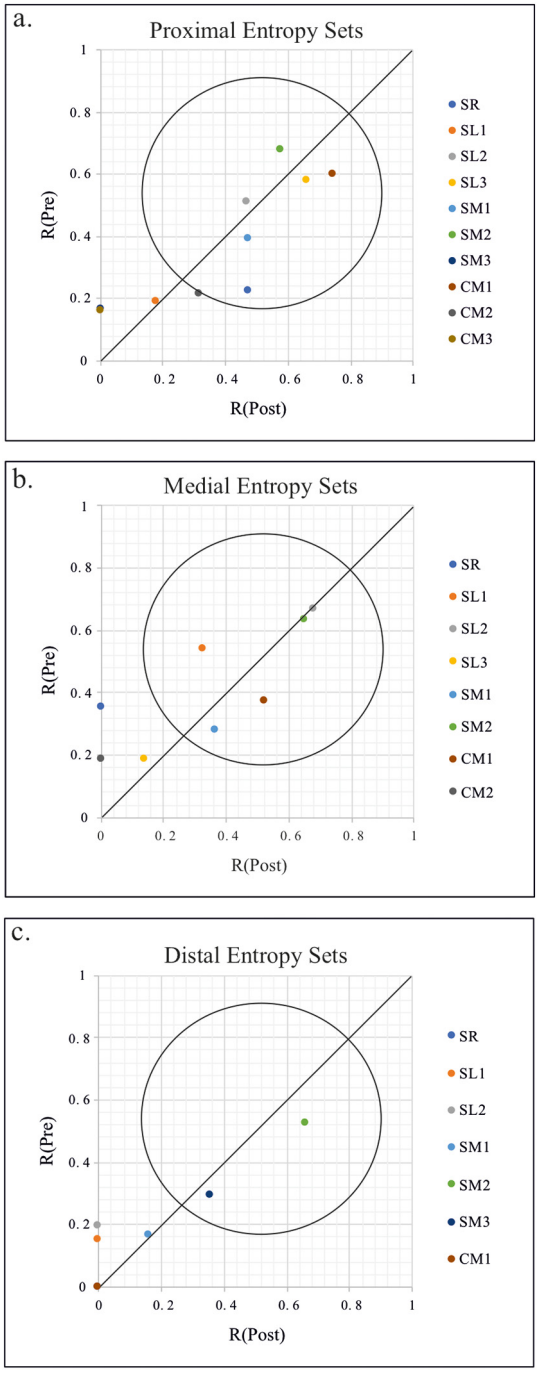

Fig. 10. Distribution of normalised entropy sets with respect to individual states for a) proximal, b) medial, and c) distal sections. The area within the circular region represents asymmetrical Type A-4 cycles of Hattori (1976).

(Fig. 3-5), and are more variable in character than those located at the base and middle of beds. Nevertheless, a general trend is observed in CB 11-3 and CB 6, where facies above the grain size break transition from SR and SL2 facies in proximal sections, respectively, to SM1 in medial sections. A similar trend is observed in CB 11-3 for the underlying facies and consists of SR facies in proximal locations, transitioning to SL2 facies downslope. The underlying facies in CB 6 is SM1 facies across the outlier.

4.4.4. Type IV grain size breaks

Type IV grain size breaks are the most common across the outlier and separate sand (750 to 88 μm) from an overlying laminated to massive

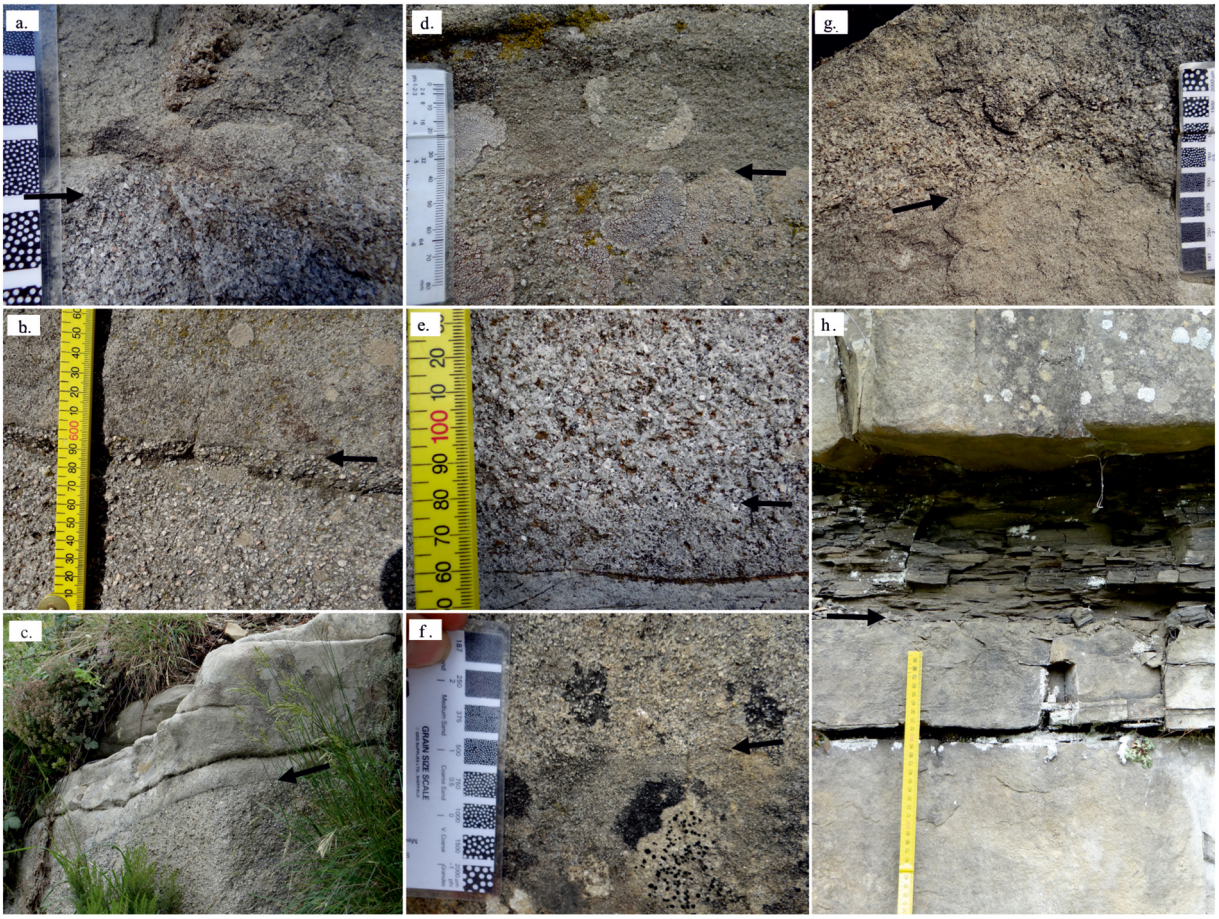

Fig. 11. Outcrop photographs illustrating the four types of grain size breaks observed in the Peïra Cava outlier. a) and b) Type I grain size breaks with >2 mm sediments below and finer sand-size sediments above. c) and d) Type II grain size with coarser sand-size sediments below and finer sand- and silt-size sediments above. e) to g) Type III grain size break with finer sediments below and coarser sediments above. h) Type IV grain size break at the top of most beds, separating silt and sand-sized sediments below and mud above.

mudstone (MM and ML) interval (Fig. 11h). They occur exclusively at the top of sandstone beds. Due to erosion and amalgamation of beds (i.e. SW and CSE), Type IV grain size breaks are less common in proximal locations compared to more distal locations. Vertically, the grain size break occurs predominantly between the SL or SR facies and ungraded mudstones (MM). Distally, there is an increased occurrence of graded massive sandstone below the grain size break (e.g. ER CB 7 and NES CB 10-2, 11-2, and 11-3).

4.5. Internal bed character, geometry, and downslope facies tract

Figs. 3 to 6 illustrate the vertical and lateral changes in the internal bed character and geometry in the eight beds. There is a progressive distal fining and thinning of all beds, and a consistently low mud content across the outlier. However, the internal bed character and geometry of individual facies along downflow transects are highly variable. Fig. 12 shows a number of downslope facies tracts that describe key changes seen in the eight beds. These facies tracts are described in terms of the vertical and lateral distribution of the massive sandstone facies. Cross-flow transects of the beds can only be acquired in distal locations from NW and NWT sections to NE and NES sections, and have been shown as part of the downslope transects and marked on Figs. 3 to 5. The cross-floor transects show similar characteristics across the outlier.

4.5.1. Facies tract I

Facies tract I is characterised by a gradual transition from graded massive sandstone in proximal and medial sections to visually ungraded massive sandstone in distal sections. The massive sandstone facies form a subordinate facies in the core of the beds in proximal and medial sections, progressively becoming the dominant facies downslope (Fig. 12a). This change in character is clearly seen in Beds CB 11-1 and CB 10-2.

In proximal sections, CM1 and SL3 facies typically underlie SM2 facies. These facies decrease in thickness towards medial sections, where they taper out and/or transition laterally into SM2 facies. The overlying facies intervals consists of SL2 and SL1. The SM2 facies gradually transitions to SM1 facies in distal locations. The structured facies interval above the SM1 and SM2 facies is thickest in proximal locations, attaining thicknesses of ~1 m before thinning progressively downflow (Figs. 3-4 and 12a). This thickness is primarily related to tapering and pinch out of the thin stratified sandstone, with the SL1 and SR facies intervals maintaining their thickness across the outlier (Fig. 12a). Centimetre-scale stratified, ordered mud clasts are present in proximal locations, passing vertically and laterally into graded dispersed mud clasts. In distal sections, mud clasts are exclusively mm-scale graded dispersed variety.

In distal sections, a Type II grain size break separates SM1 facies from the overlying SL1 and SR facies. These grain size breaks are correlated to adjacent sections in the cross-flow direction. Type II grain size breaks are also present proximal sections, but the facies above and below are more variable. SL2 facies below and SL facies above the grain size break are the most common facies.

The bed geometry has a thickness maximum in the proximal sections and closely approximates a linear (CB11-1) to sigmoidal (CB10-2) profile. For CB11-1, the proximal maximum would be the

Table 4
Characteristics of the four grain size breaks observed in the study area. An asterisk (*) above the facies code refers to the predominant facies below and above the grain size break. U - ungraded, N - normal grading, I - Inverse graded.

Bed	No of observations	Lateral position	Vertical position	Grading below	Grading above	Grain size below	Grain size above	Facies below	Facies above
Type I - gravel overlain by finer grained sediments									
CB 5	3	Proximal & medial	Base & middle	U	N	> 4 mm	1.5–1 mm	*CM1, SL3	SM1, SM2
CB 6	4	Proximal & medial	Base to top	N, U	U	6–2.5 mm	1.5 mm - 500 μm	CM1	*SM1, SL2
CB 7	3	Proximal	Base & middle	I	U	16 - 6 mm	4 - 2 mm	CM1	CM1, *SM3
CB 10-1	3	Proximal & medial	Base & middle	I, U, N	U	8 - 3 mm	1.5 mm - 500 μm	CM1	*SM1, SM3
CB 11-2	2	Proximal	Base	I, N	N	4 - 3 mm	2 - 1 mm	SL3	SL3
Type II - coarse sand overlain by finer sand									
CB 5	2	Proximal & medial	Top	N, U	N	250 - 177 μm	125 - 62 μm	SL2	SL1
CB 6	7	Proximal to distal	Top & middle	N, U	U	1.5 mm - 375 μm	1 mm - 100 μm	*SM, SL2	SM, SL1, *SL2
CB 7	4	Proximal	Top & middle	N, U	N, U	2 - 1 mm	1 mm - 125 μm	SL3	SM1, *SL1
CB 10-1	3	Proximal to distal	Top	N, U	N, U	1 mm - 375 μm	1 mm - 187 μm	SL2, *SM3	*SL1, SL2
CB 10-2	3	Proximal to distal	Top & middle	N, U	N, U	500 - 250 μm	187 - 100 μm	*SL2, SM2	*SR, SL1
CB 11-1	4	Proximal to distal	Top & middle	N, U	N, U	500 - 250 μm	250 - 125 μm	*SM, SL2	*SR, SM1
CB 11-2	1	Distal	Top	N	U	250 μm	187 μm	SL2	SL1
CB 11-3	5	Proximal & medial	Top & middle	N, U	N, U	750 - 125 μm	4 mm - 375 μm	SL1, *SR	SM1, SL2, SR
Type III - finer sand overlain by coarser sediments									
CB 6	1	Proximal & medial	Base to top	N, U	N, U	>500 μm	>750 μm	SM	SM1, SL2
CB 7	5	Proximal & medial	Base to top	N, U	N, U	4 mm - 500	6 - 1 mm	CM1, SM1	CM1, SL3, SM2
CB 10-1	2	Proximal	Base	N, U	N, U	3–1.5 mm	8 - 3 mm	CM1	SL3, CM1
CB 10-2	1	Medial	Top	N	U	125 μm	500 μm	SL1	SL2
CB 11-3	3	Proximal & medial	Top	N, U	N, U	750 - 125 μm	4 mm - 375 μm	SL1, *SR	SM1, SL2, SR
Type IV - sand overlain by mud									
CB 5	5	Proximal to distal	Top	N, U	–	88 μm	Mud	SR, ZL	MM, ML
CB 6	6	Proximal to distal	Top	N, U	–	750 - 100 μm	Mud	SL, SR	MM, ML
CB 7	6	Proximal to distal	Top	N	–	354 - 100 μm	Mud	SR	MM, ML
CB 10-1	5	Proximal to distal	Top	N	–	187 - 88 μm	Mud	SL2, SR	MM, ML
CB 10-2	7	Proximal to distal	Top	N, U	–	250 -100 μm	Mud	SR	ML
CB 11-1	5	Proximal to distal	Top	N	–	250 - 125 μm	Mud	SR	ML
CB 11-2	4	Proximal to distal	Top	U	–	250 - 125 μm	Mud	SR, SL	ML
CB 11-3	6	Proximal to distal	Top	N	–	250 - 125 μm	Mud	SR, SL, SM2	ML

minimum preserved thickness due to the partial erosion of the bed by subsequent flows (Fig. 3). Bed thickness decreases gradually across the outlier; by as much as ~75% over a distance of ~11 km. However, a less pronounced decrease (~40–45%) in bed thickness is seen between the NWT/NW and NEW sections (Fig. 3). In CB10-2, a local increase in bed thickness of ~9% is observed between NWT and NW section.

4.5.2. Facies tract II

Facies tract II consists of SM3 facies exclusively bounded by Type II grain size breaks in distal locations (Fig. 12b, c). This change in bed character is seen in CB 6, 10-1, and 11-2. The upper grain size break typically separates the SM3 facies from an overlying thin interval of SL2 and SR facies, or overlying mudstone. The lower grain size break separates an underlying CM1 facies. In a crossflow direction, the upper grain size break can be correlated between distal sections (Figs. 3-5 and 12). The SM3 facies always contains mud clasts in the core and top of the bed, with clast size varying from 4 mm to <40 cm. These mud clasts occur as nested discontinuous zones sub-parallel to bedding and may show weak grading.

Up-dip from distal sections, SM3 facies transitions abruptly to SM1 and SM2. For an ~2 m thick SM3 interval (i.e. CB 10–1), this transition occurs over a distance of 4 km (NW to NWT section; Fig. 4). Similar to facies tract I, a thin (< 20 cm) structured interval comprising SL2, SL1 and SR facies drape the massive sandstone. This structured interval thickens progressively up-dip at the expense of the underlying SM1 facies, which in turn tapers out in proximal sections. In contrast, the SM2 interval maintains or increases its thickness up-dip. In proximal sections, facies tract IIa (i.e. CB 11–2 and 10–1) and IIb (CB6) can be differentiated based on the presence of large mud and sandstone clasts in the coarser (>2 mm) grain facies underlying the SM2 interval (Fig. 12b, c). Facies tract IIa is characterised by coarser grained (>2 mm) facies that lack mud clasts. The coarser grained facies can be massive (CM1; CB 10-1) or structured into thick spaced stratification (SL3; CB 11–2). Downflow, the CM1 and SL3 facies pinch out abruptly, transitioning laterally and vertically into SM1 and SM2 facies. In contrast, facies tract IIb is characterised by very thick intervals (>3 m) of CM1 and CM2 facies with rafted, ordered stratified and dispersed graded mud and sand clasts (Fig. 12c). The interval has a highly variable geometry, doubling in thickness over a distance of ~1.5 km (between SW and SE sections), before decreasing and pinching out abruptly over 2 km (Figs. 3 and 4). The transition to the overlying SM1, SM2 and SL2 is marked by a Type I grain size break, which can be correlated downslope for a distance of ~5–6 km. Immediately up-dip of CSE section (for ~0.5 km), the clast-rich CM1 and CM2 facies transition abruptly to clast-poor CM1 and massive sandstone facies, similar to Facies Tract IIa.

Facies tract II has a thickness maximum in proximal sections. Bed thickness for facies tract IIa decreases gradually; < 40% over a distance of 11 km. A significant proportion of this thickness reduction can be related to the pinch out of the coarser grain CM1 facies, with the overlying sand grained facies maintaining a relatively uniform thickness. The downslope profile most closely resembles a linear trend, with increased rates of thinning in medial sections. In comparison, Facies Tract IIb has a more sigmoidal bed profile, with an abrupt thickness change in medial sections that amounts to as much as 71% over a distance of ~4.5 km. This is largely due to the highly variable thickness of clast-rich CM1 and CM2 intervals. Between ER and NE sections, a distance of ~3 km, Facies Tract IIb maintains a comparatively uniform thickness (+/− 10% change).

4.5.3. Facies tract III

Facies tract III consists of thick intervals of alternating SM1 and SM2 facies in medial and distal sections (Fig. 12d, e). This characteristic is clearly seen in beds CB11–3, CB7 and CB5. The SM1 facies interval are typically thicker than SM2 facies that separate them. In all beds, the proportion of massive sandstone facies, in particular SM1, increases progressively downslope (Fig. 12d, e).

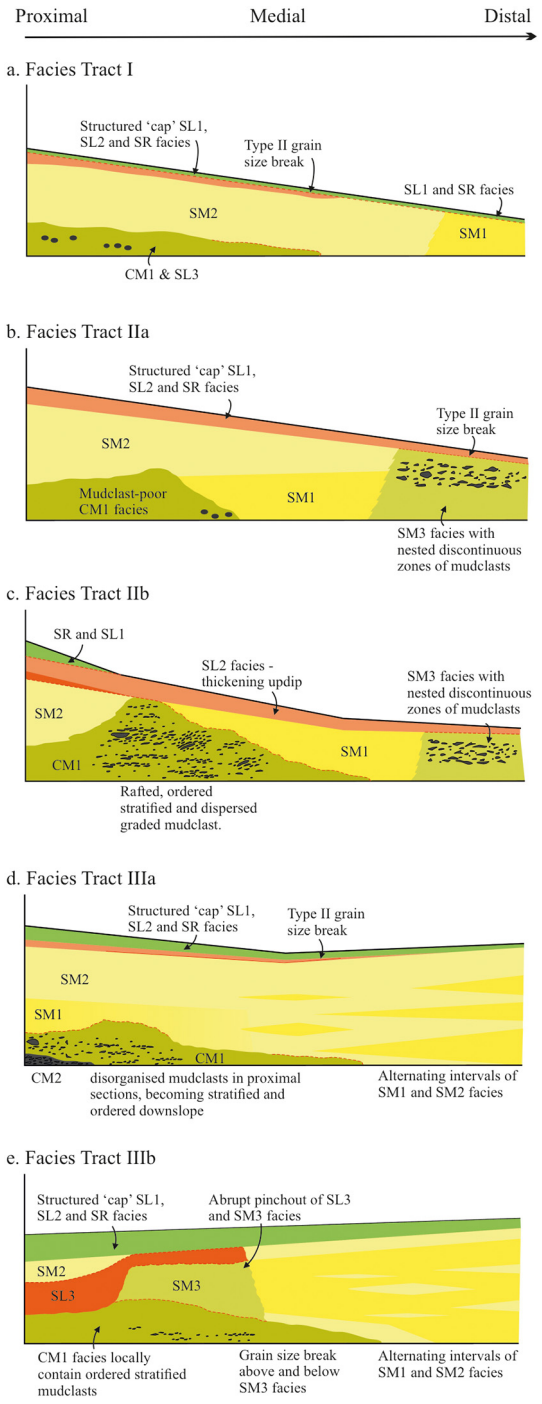

Fig. 12. Generalised facies tracts of the correlatable beds showing internal bed character. Due to the high sediment facies variability between sections in proximal locations, only the most common characteristics between beds are incorporated in the facies tracts. Beds thickness changes are illustrative, not quantitative, and show overall trend in downslope variation.

In distal sections, these massive sandstones are capped by thin intervals of SL1 and SR facies without an intervening grain size break. However, up-dip, this transition is separated by a Type II grain size break with the underlying facies typically SM2 and SL2. Moving up-dip, the structured cap progressively thickens at the expense of the massive sandstone interval, which in turn is gradually underlain by thicker intervals of CM1 and/or SL3 facies. Thus, the alternating SM1 and SM2 intervals form the core of the beds in medial and proximal sections. The transition between the CM1 and/or SL3 facies is sharp, marked by either a Type I grain size break or a short strongly graded interval. The CM facies in proximal locations contain mm to cm, and locally dm-scale mud clasts. They occur as disorganised rafted clasts in most proximal locations, evolving downslope to more organised ordered stratified and/or dispersed graded variety. The former variety is closely associated with locations of internal grain size breaks and erosive scours (Fig. 12d). The mudclast interval pinches out abruptly over a distance of 2 km.

In proximal sections, facies tract III can be differentiated into Type IIIa (CB11-3 and CB5) and IIIb (CB7) based on the presence of SM3 and SL3 facies (Fig. 12d, e). Facies fract IIIa lacks the massive sandstone with patchy texture, and instead the graded and ungraded massive facies are dominant. Vertically, the two facies are more organised such that beds lack the cyclic transitions seen in medial and distal sections (Fig. 12d). In contrast, facies tract IIIb is characterised by a lateral transition from SM1 and/or SM2 to SL3 and SM3 facies. The latter facies has foundered into the underlying CM1 facies and is separated by a Type I grain size break. The SM3 facies is also separated from the overlying SL3 facies by a grain size break. Both of these grain size breaks can be correlated between proximal sections. Up-dip, the SM3 facies pinches out abruptly over ~0.5 km, with the SL3 facies overlying the CM1 facies in the most proximal sections (Fig. 12e).

Bed geometry of facies tract IIIa has accentuated highs in proximal and distal sections. Bed thicknesses decrease by ~40% from the proximal to medial sections, but increase again in distal sections to within +/− 10% of the thickness maximum observed up-dip (Fig. 6). In comparison, facies tract IIIb also has accentuated proximal and distal highs, with only minor decrease (~-15%) in bed thickness in medial sections (Fig. 5). However, distal bed thicknesses are marginally larger (+10–15%) relative to proximal sections.

5. Discussion

5.1. Formation of massive sandstone at single sections

The massive character in deep-water deposits has been considered a manifestation of static suspension settling, suspension fallout without traction, incremental deposition from near bed layers or sustained near bed liquefied zones within quasi-steady or surge type turbidity currents (Lowe, 1982; Arnott and Hand, 1989; Kneller and Branney, 1995; Stow and Johansson, 2000; Sumner et al., 2008; Cantero et al., 2012a; Dorrell et al., 2013). Alternatively, non-cohesive to cohesive debris flows are also envisaged to produce a massive deposit (Lowe, 1976; Shanmugam, 1996; Baas et al., 2009; Sumner et al., 2009; Talling et al., 2012). These depositional processes are now contextualised with respect to the empirical evidence and statistical analysis presented in this study. For interpretation of depositional processes for the remaining facies, please refer to Table 1.

5.1.1. Ungraded, massive sandstone (SM1)

Ungraded massive sandstones have commonly been ascribed to deposition from a sustained liquified zone beneath turbidity currents and non-cohesive debris flows (Lowe, 1982; Kneller and Branney, 1995; Shanmugam, 1996; Talling et al., 2013). The Markov chain and entropy analysis in proximal and medial sections reveal a degree of dependence for the SM1 facies with the underlying CM and SM2 facies, while in distal sections it exerts a strong influence on the succeeding SM2 facies. The common occurrence of a Type I grain size break between the conglomeratic and ungraded massive sandstone in proximal locations impedes extrapolation of hydrodynamic processes upwards. Nevertheless, the presence of a Type I grain size break does indicate that the flow was bi-partite with a highly concentrated basal layer and a lower concentration upper layer (see Section 5.2.1).

Regardless, the gradual transition from SM2 to SM1 facies in proximal sections, as well as the opposite trend in distal sections, may provide evidence for the formation of SM1 facies. These transitions have been observed in physical and numerical experiments involving

relatively high-sediment concentration. Static settling experiments show efficient grain segregation at <20% volume concentration to generate a strongly graded massive sandstone, while frictional interlocking of grains is shown to inhibit segregation processes at >50% volume concentration (Amy et al., 2006). Similar settling behaviour are also observed in the flume experiments where sediment concentration in excess of 45% fully suppressed turbulence in a grain friction dominated basal layer, leading to the development of ungraded deposits (Breien et al., 2010; Cartigny et al., 2013). At intermediate concentrations (ca 20–45%), experimental studies have shown hindered settling to produce ungraded to poorly graded deposits (e.g. Amy et al., 2006; Sumner et al., 2008; Dorrell et al., 2011; Dorrell et al., 2013). Though these studies reported disparate grain support mechanisms, they all support incremental deposition from a high concentration near bed layer (sensu Vrolijk and Southard, 1997) where grain segregation was inhibited based on sediment concentration. These near bed layers are fed and driven by an overriding turbulent flow and deposition occurs from the base-upwards due to interlocking of grains (Hiscott, 1994b; Cartigny et al., 2013).

5.1.2. Graded, massive sandstone (SM2)

The Markov chain and entropy analysis in the three groupings indicate that the successor facies (i.e. SL2 facies) are non-random and there is a strong dependence on the graded massive sandstone. This transition, along with the normal grading (at the very least in the SM2 facies), implies that flow velocity and concentration were decreasing during and succeeding deposition of the SM2 facies (Sumner et al., 2008). It is therefore unlikely that graded massive interval were deposited by a sustained near bed liquefied zone, which requires a constant, prolonged and rapid sediment fallout (sensu stricto Kneller and Branney, 1995). In addition, these types of flows have not yet been recreated experimentally. In contrast, experimental flows have shown the formation of SL2 facies to be related to lateral shearing of grains during repeated collapse and subsequent erosion of near bed layers (Arnott and Hand, 1989; Vrolijk and Southard, 1997; Leclair and Arnott, 2005; Sumner et al., 2008; Cartigny et al., 2013). However, the deposit character depends on the concentration (~10 to 35%) within the near bed layers, which in turn depends on the sediment fallout rates from the overriding flow (Sumner et al., 2008; Cartigny et al., 2013). At lower concentrations, turbulent reworking of collapsing laminar sheared layers produced the SL2 facies (Vrolijk and Southard, 1997; Sumner et al., 2008; Cartigny et al., 2013). At higher concentrations, stratification is seen to be suppressed leading to the development massive deposits. The bed aggradation rates at which this occurs is reported to be greater than 2.64 cm min^{-1} (Arnott and Hand, 1989; Sylvester and Lowe, 2004; Sumner et al., 2008). Thus, extrapolating the hydrodynamic interpretation of the structured facies down to the massive sandstone, as advocated by the vertical transitions, supports the formation of graded, massive sandstone by repeated collapse of near bed layers (similar to ungraded massive sandstones but with a lower concentration).

5.1.3. Massive sandstone with patchy texture (SM3)

Most intervals of SM3 facies are located in distal sections of the outlier. They have previously been described by Talling et al. (2013) in the Marnaso-Arenacea Formation in the northern Apennines, and attributed to deposition from liquefied debris flows from which sand grains partially settle out. Experimental studies on subaerial and subaqueous debris flows have shown the development of a transient excess pore pressure by gravitational loading, which can support grains during transport (Iverson, 1997; Major and Iverson, 1999; Major, 2000; Ilstad et al., 2004; Breien et al., 2010; Kaitna et al., 2016). Dissipation of this pore pressure during transit and deposition of the debris flow may mobilise sediments via slow convection and elutriation. A physical expression of this could be the irregular or patchy texture in the massive sandstone. However, to date no experimental work has reproduced this textural characteristic.

The presence of chaotically organised, unsegregated mud clasts towards the middle and top of the SM3 facies, as well as a sharp grain size break at the upper boundary, does lend support to deposition from debris flows (Talling et al., 2012). These mud clasts can be supported in debris flows if they are less buoyant and have lower densities than the matrix (Postma et al., 1988). The fact that they are unarmoured suggests mud clasts may have been protected by a surrounding debris flow (Piper et al., 1999; Li et al., 2017; Hizzett et al., 2020). The irregular shape of mud clasts also implies that they experienced less abrasion as is common in debris flows (Fukuda and Naruse, 2020).

However, the crude normal grading identified in the SM3 facies from thin sections eludes to deposition from a turbulent flow. Notwithstanding this fact, experimental studies have also shown crude coarse-tail grading occurring in debris flows after the flow has stopped moving (Major, 2000; Baas et al., 2009; Sumner et al., 2009; Baas et al., 2011). This could be related to the hydraulic diffusivity of the debris flow, which may promote weak grain segregation. In a more permeable debris flow, fluid pore pressures and effective stresses change more rapidly due to the presence of

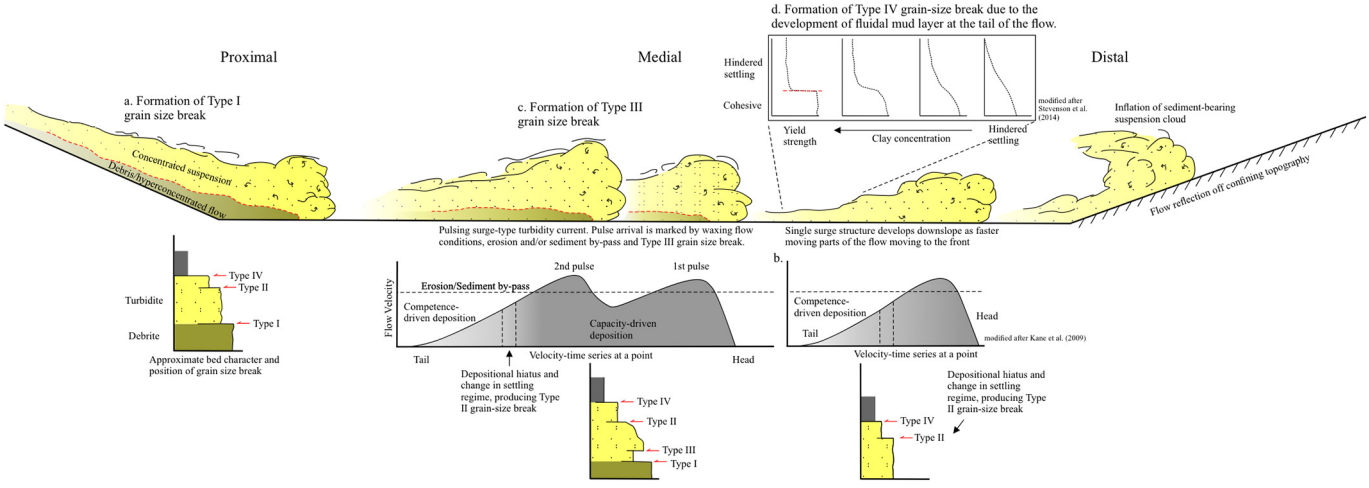

Fig. 13. Models showing the development of grain size breaks in the Peïra Cava Basin. a) Type I grain size break is created by en-masse freezing of the lower layer and sediment reworking the overlying turbulent layer. Further downslope, the hyper-concentrated basal layer transforms into a turbulent flow. b) Type II grain size break represents change in settling regime within a turbulent flow from capacity to competence driven deposition. c) Type III grain size break is created by multiple surges within a single flow. Each surge is characterised by waxing conditions, during which earlier deposited sediments may be eroded. Return to net deposition may lead to sedimentation of coarser sediments. d) Type IV grain size break is created by sediment bypass within fluid mud layers.

pervasive pathways for fluid migration. As the pore pressure dissipates, the deposit undergoes consolidation from the base upwards (Sumner et al., 2009; Baas et al., 2011). The simultaneous expulsion of the pore fluid elutriates finer grains, while coarse grains settle under hindered settling, producing a crudely graded interval. This latter explanation for the normal grading observed in facies SM3 could have also led to the formation of patchy texture. Thus, supporting the mechanism proposed by Talling et al. (2013) for the deposition of massive sandstone with patchy texture.

5.2. Origin of the grain size breaks

The eight beds contain four different types of grain size breaks. Local seabed topographic obstacles are not considered likely to create these grain size breaks due to the inferred flat intra-basin floor topography (Sinclair and Cowie, 2003; Aas et al., 2010). In the following section, they are interpreted as a product of sediment transport and depositional processes (Fig. 13).

5.2.1. Type I grain size break

Type I grain size breaks are predominantly confined to proximal and medial locations. Based on experimental and field observations, they are interpreted to represent a sharp rheological transition between a highly concentrated basal layer and an overriding lower concentration plume (Sanders, 1965; Postma et al., 1988; Mutti et al., 1999; Tinterri et al., 2003; Ilstad et al., 2004; Stevenson et al., 2014). In the present study, the dominant facies beneath Type I grain size breaks are conglomeratic facies, which are likely to be deposited by debris flow or inflated sandflow (Table 1; Hiscott, 1994b; Sohn, 1997, Pickering and Hiscott, 2015). In contrast, the overlying facies, commonly massive or stratified sandstones, are more indicative of incremental deposition from an overriding turbulent current (see above). Due to the rapid deposition of both facies with only short periods of sediment by-pass, Type I grain size breaks not only represent a rheological transition, but also likely preserve the vertical bipartite structure of the flow in the deposit (Fig. 13a). The lateral correlation of the grain size break in proximal location can thus be used to infer the runout distance of the basal dense layer. In the case of CB6, this distance is ~2 km. Beyond the proximal sections, the observations indicate that flows decoupled and deposited massive sandstones as they travelled downslope.

5.2.2. Type II grain size break

Type II grain size breaks are common in the Peïra Cava outlier, observed in most beds in proximal to distal sections. They are here interpreted to represent a transition from capacity- to competence-driven deposition (Fig. 12b; Kneller and McCaffrey, 2003; Stevenson et al., 2014). In experimental studies, this transition in settling regime is often associated with sediment by-pass, reworking and/or erosion of earlier deposited sediments (Vrolijk and Southard, 1997; Sumner et al., 2008; Cartigny et al., 2013). The sediments below the grain size break are poorly graded and sorted, while those above show strong grading and improved sorting. The field study of Tinterri et al. (2016) and Cunha et al. (2017) also interpreted similar facies and concomitant grain size break as a by-pass horizon due to the decoupling of the basal dense flow and upper turbulent flow. In the current study, facies below the grain size break are either massive or stratified intervals of poorly sorted sandstones. These facies are deposited incrementally by collapsing high-concentration near bed layers in which hindered settling is active (Arnott and Hand, 1989; Hiscott, 1994a; Sohn, 1997; Leclair and Arnott, 2005; Sumner et al., 2008; Dorrell et al., 2011; Cartigny et al., 2013). Above the grain size break, possibly after a period of bypass, sediment sorting improves and deposits are commonly strongly graded, indicating enhanced grain segregation processes (likely a decrease in hindered settling and an increased in elutriation) due to reduced sediment fallout rates (Table 1; Amy et al., 2006; Baas et al., 2011; Dorrell et al., 2011; Talling et al., 2012; Tinterri et al., 2016, 2017; Cunha et al., 2017). The cause of the transition from capacity- to competence-driven deposition could be related to longitudinal variation in flow concentration and velocity (Kneller and McCaffrey, 2003) or flow deceleration due to topographic confinement (Tinterri and Muzzi Magalhaes, 2011; Tinterri et al., 2016; Cunha et al., 2017).

5.2.3. Type III grain size break

Type III grain size breaks are located only in proximal and medial sections. They are surmised to form from waxing flow conditions that become sufficiently energetic to increase the capacity of the flow and erode the previously deposited sediments (Fig. 12c; Kneller, 1995; Kneller and McCaffrey, 2003). The overlying coarser material is in turn deposited under conditions of increaseing turbulent energy and shear velocity (i.e. waxing flow conditions) (Sylvester and Lowe, 2004; Sumner et al., 2012; Stevenson et al., 2014). Such conditions may arise if the flow is surging (i.e. pulse of rapidly moving fluid) at the source due to retrogressive slope failures, variations in ground shaking in currents initiated by single seismic events, variations in flood hydrograph for hyperpycnally generated flows, or internal waves generated by interaction with topography and/or velocity pulses (Piper et al., 1999; Mulder and Alexander, 2001; Kneller and McCaffrey, 2003; Patacci et al., 2015; Ho et al., 2018). In the current study, no inverse grading is seen in the facies underlying Type III grain size breaks to conclusively indicate waxing flow conditions, which intimate flows were either steady or waning prior to the formation of the grain size breaks (Kneller, 1995). Notwithstanding this observation, it is likely that increased flow shear velocities and turbulence intensities completely removed the depositional record of the waxing phase.

Furthermore, the predominantly proximal occurrence and discontinuous nature of the grain size break suggest that the flows were highly unsteady and pulsatory (i.e. dominated by multiple surges characterised by waxing and waning conditions) near the source (Kneller and McCaffrey, 2003). Regardless of the origin of the pulsating flow, the complete absence of the grain size break in distal locations implies flows likely developed a simple surge structure that was depletive and waning (Ho et al., 2018). The relative small size of the Peïra Cava outlier also implies that such organisation occurred over a relatively short distance (~6 km).

5.2.4. Type IV Grain size break

Type IV grain size breaks mark a vertical transition from non-cohesive sand and silt to mud. They are interpreted as the onset of cohesive behaviour in the tail of the flow as clay and other cohesive material settle out (Piper, 1978; Macdonald, 1986; Amy, 2000; Gladstone and Sparks, 2002; Remacha et al., 2005; Kane et al., 2007; Sumner et al., 2012; Stevenson et al., 2014). This leads to the development of high concentration fluid mud layers that hinder non-cohesive grain settling (Baas et al., 2014; Stevenson et al., 2014). As the fluid layers move downslope, they transport grains size fractions that would otherwise settle out of suspension, thus creating the grain size break (Fig. 12d; Baas and Best, 2002; Baas et al., 2009; Sumner et al., 2009; Baas et al., 2014; Stevenson et al., 2014).

5.2.5. Implication of the grain size breaks

The presence of multiple Type I, II and, III grain size breaks and their lateral distribution indicates that flows were stratified, unsteady and pulsatory in nature. At a given point, this translates into phases of waxing and waning flow velocity and sediment concentration. In proximal and medial sections, beds are influenced more by the surging head (and subsequent surges), leading to greater sediment re-entrainment and/or by-pass. Massive sandstones in these locations are likely to form part of sequences of facies and bounded by grain size breaks. Further downslope, the type and frequency of grain size breaks indicate flows became more organised. Here the massive sandstone are less likely to be bounded by grain size breaks and more likely to constitute the sole facies within the beds.

5.3. Vertical facies transition

Chi-squared statistics reject the null hypothesis of quasi-independence at the 99.5% confidence level for the proximal and distal groupings, and at the 97.5% for the medial grouping. These results generally concur with the entropy analysis, which show no cases where E(Pre) ≈ E(Post) ≠ 0 (Table 3), implying some level of dependency of one state on another. Both the Markov and entropy analysis therefore support in a statistical manner the conclusion that deposition of the various facies in the eight beds depend on temporally evolving flow conditions. This analysis is therefore used to infer temporal evolution of flow processes and deposition of massive sandstone facies in the Peïra Cava outlier.

5.3.1. Proximal Locations

In proximal locations, the preferred vertical transition show both SM1 and SM2 facies occupy a position in the middle of the bed (Fig. 9). They are overlain by structured intervals and underlain by SL3 or CM facies. This facies sequence broadly conforms with the vertical transition described by Hiscott and Middleton (1979), Lowe (1982), Mutti (1992) and Mutti et al. (2003), and was interpreted as a deposit of surge-type bipartite flows. However, a key deviation from the models in the present study is the repetition or incomplete sequences seen in the top half of the bed, and the presence of grain size breaks. The grain size breaks commonly separate massive sandstones from the underlying and overlying facies (Fig. 12), and suggest the flow had multiple surges which created phases of waxing and waning flow velocity and concentrations (Fig. 13).

In the present study, the CM and SL3 facies at the base are likely to be transported by high concentration traction carpets and/or debris flow processes and deposited rapidly (Table 1; Hiscott, 1994b; Sohn, 1997; Mulder and Alexander, 2001; Pickering and Hiscott, 2015). The overlying SM1 and SM2 facies were deposited by high concentration near bed layers beneath a turbulent flow. Above the SM1 and SM2 facies, the ideal vertical transition is SL2, SL1 and SR facies. With the exception of SL2 facies, which were deposited in a manner similar to the massive facies, the SL1 and SR facies were formed by grains reworked as bedload in a lower flow regime (Allen, 1982; Baas, 1999; Leclair and Arnott, 2005; Sumner et al., 2008; Talling et al., 2012). This sequence broadly resembles the modified Bouma sequence of Talling et al. (2012), and is interpreted to be deposited by turbidity currents. Thus, the boundary between a high- and low- concentration turbidity current can be placed between the transition from SL2 and SL1 facies (Talling et al., 2012). This transition is commonly recognised by a grain size break, and marks a switch from capacity- to competence-induced deposition as a result of longitudinal gradient in velocity and sediment concentration (Kneller and McCaffrey, 2003; Stevenson et al., 2014). Alternatively, the sequence and grain size break can be related to rapid deceleration induced by topographic confinement in proximal locations (Tinterri and Muzzi Magalhaes, 2011; Tinterri et al., 2016; Cunha et al., 2017). In such a scenario, the facies sequence could be result of a complex interplay between waxing and waning conditions, and capacity-driven deposition (basal massive sandstone) with concomitant development of turbulent energy and competence-driven deposition induce by flow deceleration due to flow-topography interaction (Tinterri and Muzzi Magalhaes, 2011). Regardless of the exact mechanism, the overall structure of the deposits in proximal locations preserves the vertical structure of a bipartite flow, as well as a transition from high concentration but turbulent flow to a lower concentration, turbulent flow (Postma et al., 1988; Sumner et al., 2008; Stevenson et al., 2014; Tinterri and Muzzi Magalhaes, 2011).

5.3.2. Medial locations

Based on the observed transitions, a sequence consisting of a thin interval of coarser grained facies (e.g. CM1) at the base, followed by SM1 and/or SM2 and structured facies at the top is the most common sequence seen in medial sections. This sequence is similar to proximal locations, and suggest similar temporal evolution of flow processes. However, a repetitive occurrence of massive and structured intervals is indicated statistically (Fig. 9), and observed at different stratigraphic heights in beds CB11–3, CB7 and CB5 (Figs. 3 to 6). This sequence is used as a diagnostic feature of facies tract III (Fig. 12), and likely contributed to the rejection of the null hypothesis at the higher confidence level (i.e. 99.5%) in the medial sections as a whole. These repetitive sequences have not been described in previous idealised models. Longitudinal variations in flow concentration and velocity induced by surging flows may explain their formation. The passage of these surges could produce fluctuations in sediment fallout rates, and consequentially deposition of repetitive sequences of massive (ungraded and graded) and thin spaced stratified intervals (Kneller and McCaffrey, 2003). The local presence of Type II and III grains size breaks does lends supports to this mechanism (Kneller and McCaffrey, 2003; Stevenson et al., 2014). As the surges progress downslope, they cannibalise slower moving surges and the flow organises itself into a single surge (Ho et al., 2018). However, the presence of repetitive sequences in facies tract III in distal locations suggests this was not the case, and that alternative mechanisms likely created the observed internal character.

Repeating sequences of normal graded massive, laminated and/or rippled sandstones have been observed in confined basins similar to the Peïra Cava sub-basin, where they are interpreted as a record of flow interaction (i.e. reflection and deflection) with the confining topography (Haughton, 1994; Sinclair, 1994; Kneller and McCaffrey, 1999; Felletti, 2002; Muzzi Magalhaes and Tinterri, 2010; Tinterri and Muzzi Magalhaes, 2011; Tinterri et al., 2016; Tinterri and Piazza, 2019). Additional criteria for flow interaction with confining topography include opposing ripples, convulate lamination and soft-sediment deformation with load structures, and hummocky type structures (Muzzi Magalhaes and Tinterri, 2010; Tinterri and Muzzi Magalhaes, 2011; Tinterri et al., 2016; Tinterri and Piazza, 2019). However, in the current study, most beds lack many of these structures that would otherwise conclusively support flow interaction with confining topography. The proximity to the confining topography is also uncertain for medial sections.

Alternatively, the repetitive facies of facies tract III is here interpreted as a record of continuous flow interaction with the confining topography which resulted in the generation and propagation of internal waves (Fig. 14; Pantin and Leeder, 1987; Kneller et al., 1991; Edwards et al., 1994;; Muzzi Magalhaes and Tinterri, 2010; Patacci et al., 2015; Tinterri et al., 2016). In this sense, internal waves are oscillations that arise from perturbations of the hydrostatic equilibrium along density interfaces, where the balance between the buoyant restoring forces and inertial driving forces is governed by the Richardson number (Kneller et al., 1991; Tinterri et al., 2016). They record the propagation of energy, which in turn creates fluctuations in flow velocity, concentration, pressure and sediment fallout rates (Nemec, 1995; Muzzi Magalhaes and Tinterri, 2010; Patacci et al., 2015). Tinterri et al. (2016) suggested different types of internal waves can generate depending on the deceleration rate of the flow against the confining topography, from weak internal waves where there is a transference of energy, to stronger bores that have the characteristics of density currents capable of transporting and resuspending sediments. Consequentially, the characteristics of the internal waves will influence the deposit character (Muzzi Magalhaes and Tinterri, 2010; Tinterri and Muzzi Magalhaes, 2011; Patacci et al., 2015; Tinterri et al., 2016). The impact on the deposit character is likely to be greatest near the source of the internal waves where they have the greatest energy and amplitude (Edwards et al., 1994; Patacci et al., 2015; Tinterri et al., 2016; Cunha et al., 2017). Here, the deposit structure may be characterised by repetitive internal erosion surfaces, traction structures, undulate laminations, and soft-sediment deformation (Kneller et al., 1991; Kneller and McCaffrey, 1999 Muzzi Magalhaes and Tinterri, 2010; Tinterri et al., 2016; Cunha et al., 2017). With distance from the source, the waves

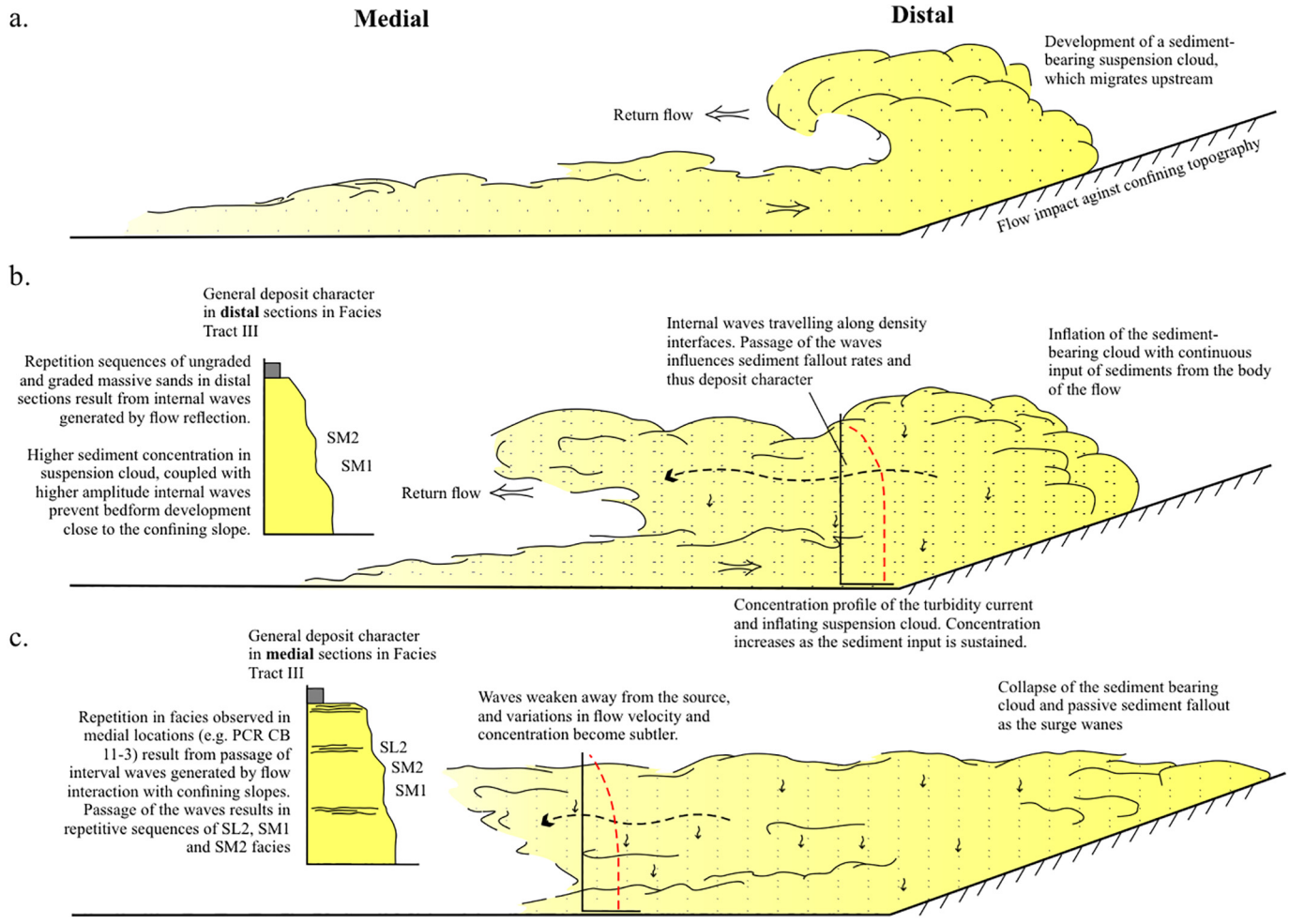

Fig. 14. Formation of a sediment-bearing suspension cloud and internal waves as a result of flow interaction with the distal confining topography. Continuous supply of sediments from the flow inflates the plume and migrates upstream. The corresponding increase in concentration results in deposition of massive sandstones in medial and distal sections. The generation and upstream passage of internal waves at density interfaces also creates fluctuations in flow velocity and sediment fallout rates, which are expressed in the deposit as repetitive sequence of facies (represented in facies tract III). Red line shows the evolution of the concentration profile of the suspension plume spatially and vertically. (For interpretation of the references to colour in this figure legend, the reader is referred to the web version of this article.)

decay and variations in flow velocity, concentration, pressure and sediment fallout rates become subtler (Muzzi Magalhaes and Tinterri, 2010; Patacci et al., 2015; Tinterri et al., 2016). This will translate into subtler facies transitions such as repeating facies of ungraded and graded massive sandstone, and thin spaced laminae (Muzzi Magalhaes and Tinterri, 2010; Tinterri and Muzzi Magalhaes, 2011; Patacci et al., 2015; Cunha et al., 2017). Such a mechanism is here interpreted as the cause of the repetitive facies observed in the medial section. However, it is difficult to ascertain the source of the internal waves (i.e. proximal, lateral slope or bounding slope). The lack of repetitive internal divisions in proximal deposits intimate flow reflection or deflection off lateral or bounding confining topography as the cause (Fig. 14).

5.3.3. Distal locations

In distal sections, the dominant facies is the massive sandstone in all the beds. These are overlain by thin intervals of structured facies (e.g. SL or SR), commonly separated by a Type II grain size break. This ideal sequence is seen in many distal basin locations and is similar to that described by Bouma (1962) Lowe (1982), Mutti (1992) and Kneller and McCaffrey (2003). It has been interpreted as a deposit of turbidity currents that experienced a switch from capacity- to competence-induced deposition. Where the SM3 facies is overlain by structured facies, this transition is always marked by a grain size break. This sequence is similar to one observed by Talling et al. (2013), who interpreted a dilute flow reworking the top of the massive sandstone. In this case the SM3 facies is interpreted to be deposited by a liquefied debris flow (Talling et al., 2013).

Similar to the medial sections, the statistical analysis indicates the presence of repetitive trends in the form of alternating SM1 and SM2 facies. These trends are clearly seen in beds CB11–3, CB7 and CB5 of facies tract III. They have not been incorporated into previous facies models, but due to their similarity with the medial sections, the trends are interpreted to form in a comparable manner i.e. flow processes associated with the interaction of internal waves. However, in this setting it is likely the internal waves were generated by the flows impacting the bounding topography due to its proximity (Fig. 14). The passage of these internal waves in turn leads to fluctuations in sediment fallout rates to the static bed (Patacci et al., 2015), and the development of alternating repetitive occurrence of ungraded and graded massive sandstones.

6. Lateral distribution of massive sandstones

In many field studies of high-density turbidites in ancient systems, a systematic downflow trend has been observed in facies architecture. The proximal (upstream) deposits comprise thick beds of massive and/or stratified sandstone capped by a thin low-density turbidite interval of finer-grained laminated and rippled sandstone (Tb to Td turbidite divisions). In distal (downflow) deposits, the massive/stratified HDT interval thins and is replaced by the LDT interval as the dominant facies (e.g. Hirayama and Nakajima, 1977; Macdonald, 1986; Tokuhashi, 1989;

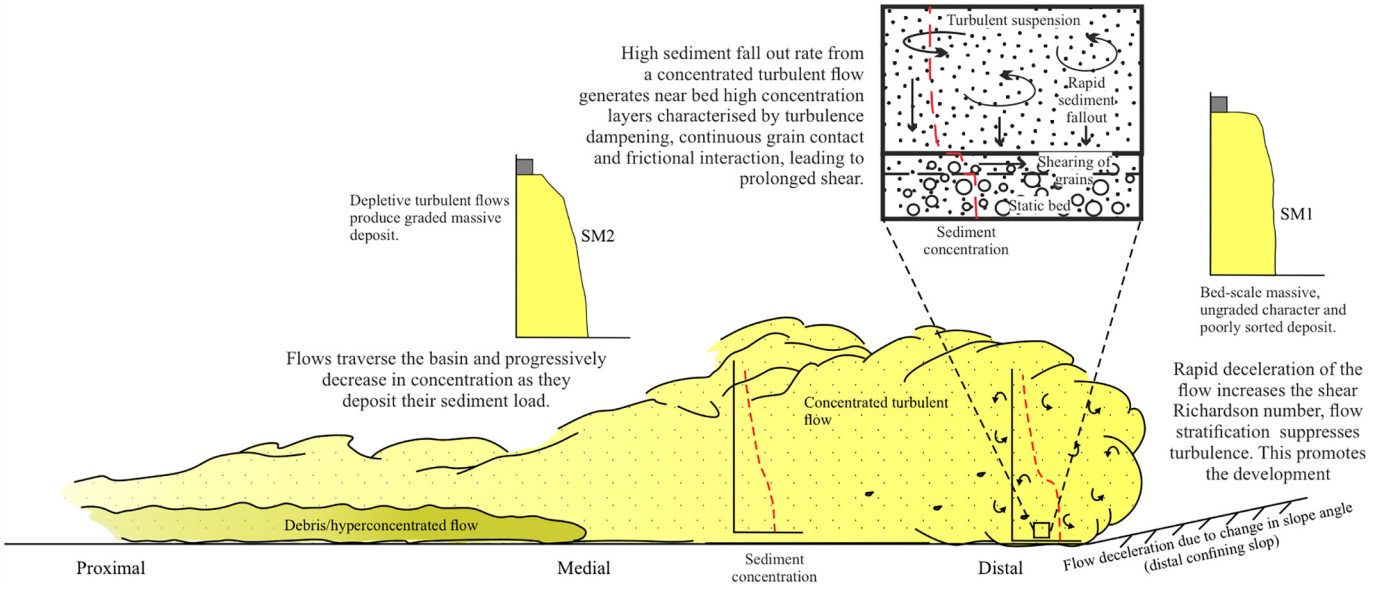

Fig. 15. Model showing the formation of ungraded massive sandstone in distal locations in facies tract I. As the flow decelerates against confining topography, it experiences increased vertical flow stratification and turbulence suppression. A denser sediment suspension near the base of the flow influences the development of high concentration near bed layers and the deposition of massive sandstone.

Remacha et al., 2005; Amy and Talling, 2006; Mcintosh, 2007; Talling et al., 2007a; Sumner et al., 2012; Talling et al., 2013; Malgesini et al., 2015; Cunha et al., 2017). These trends have also been reproduced in physical and numerical experiments (e.g. Dade et al., 1994; Tinterri et al., 2003; Baas et al., 2004; Malgesini et al., 2015), and are diagnostic of depletive and waning high density turbidity currents that experience hindered settling from a dense near-bed flow in proximal and medial settings (Talling et al., 2007a; Malgesini et al., 2015).

In the current study, the beds in proximal and medial settings are indeed predominantly composed of massive and/or thick to thin stratified intervals. However, and in contrast to the thin drape seen in other locations, the upper low density turbidite deposit locally constitute a third of the thickness of the beds, especially in proximal locations (Fig. 12). Furthermore, the facies tracts clearly show an increase in the relative proportion of the massive facies distally, while the low density turbidite intervals pinch out (Fig. 12). Similar transitions in Eocene turbidite beds on Spitzbergen were attributed to collapse of a flow due to buoyancy reversal (Plink-Björklund and Steel, 2004). The Peïra Cava outlier has been interpreted as a delta-fed turbidite, which could create ideal conditions for buoyancy reversal in the flows if the interstitial fluid suspending the sediments was of lower density. However, the observed vertical facies transitions are different to those predicted for flows with buoyancy reversal (Stevenson and Peakall, 2010; Steel et al., 2017). In the following sections, these trends are explained by flow interaction with the confining topography.

6.1. Facies tract I

Facies tract I displays a basinward transition to SM1 facies (Fig. 12a). This lateral transition is here interpreted as a response to rapid deceleration of the turbulent flow as it interacted with the confining slope (i.e. increased slope angle). Dimensionless parameters that modulate turbulence and thus the degree of turbulence dampening are the shear Richardson number and the fall velocity (Cantero et al., 2009, 2012a, 2012b). If the turbulent flow rapidly decelerated due to an increase in slope angle, the shear Richardson number would increase significantly. This in turn would lead to increased vertical flow stratification and turbulence suppression (Talling et al., 2007b). A denser sediment suspension would form near the base of the flow and influence the development of high concentration near bed layers. As flows traversed the Peïra Cava sub-basin, they are likely to be depletive and evolve to deposit low density turbidites (i.e. Tb to Td facies) as sediment concentration decrease. However, a change in slope angle could reconcentrate the flow and allow deposition of SM1 facies of facies tract I in distal locations (Fig. 15). Such a reconcentration of the flow could also be aided by the formation of a suspension cloud as the head of the flow impacted against the confining slope (Patacci et al., 2015).

6.2. Facies tract II

Facies tract II is defined by basinward transition from SM1 or SM2 facies to SM3 facies, with the latter interpreted to be deposited by liquefied debris flows (Talling et al., 2013). Experimental studies have shown the ability of small volumes of clay (~ 3–4 wt%) to modulate turbulence and modify the settling regime within flows (Baas and Best, 2002; Baas et al., 2009; Baas et al., 2011; Baas et al., 2016; Sumner et al., 2009). The clay may be introduced into the flow through erosion of a muddy substrate and/or disintegration of mud clasts (Amy et al., 2006; Ito, 2008; Davis et al., 2009; Haughton et al., 2009; Kane and Pontén, 2012; Patacci et al., 2014; Hizzett et al., 2020). The presence of unarmoured mud clasts and mud content up to 10% in the SM3 facies, compared to the SM1 and SM2 facies, does intimate incorporation of mud in to the flow through this process. In experimental studies, increasing clay concentration is shown to produce a liquefied basal layer behind the head of an erosive and turbulent flow (Marr et al., 2001; Breien et al., 2010). These liquefied layers are characterised by transient excess pore pressure and laminar behaviour, with sediments 'floating' freely in the sediment-fluid mixture (Breien et al., 2010). A downslope transformation from a turbidity current to such a flow is postulated to account for SM3 facies in distal locations (Fig. 16). Flow transformation could have been initiated by a change in slope angle, which rapidly decelerated the flow and modulated settling behaviour (Baas et al., 2009; Sumner et al., 2009). The turbulent plume that follows this phase reworks the top of the deposit to produce the grain size break and the thin interval of traction structures that commonly cap SM3 facies in distal sections.

6.3. Facies tract III

Facies tract III exhibits bed profiles with accentuated highs in the proximal and distal sections, as well as repetitive alternation of SM1,

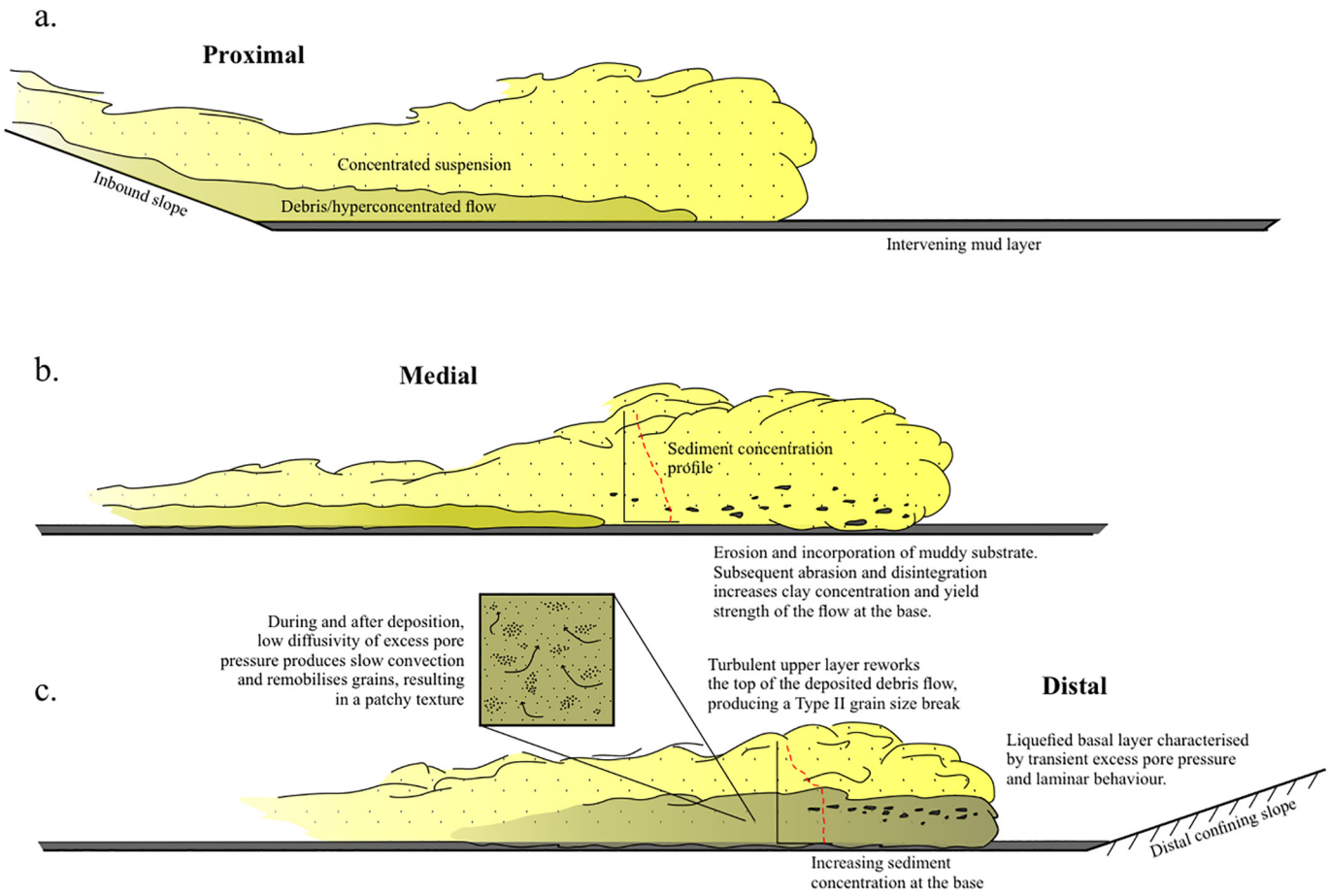

Fig. 16. Model showing the formation of the massive sandstone with patchy texture in facies tract III. An initially erosive flow entrains mud from a muddy substrate and/or disaggregation of mud clasts, leading to increased clay content in the flow. This creates a liquefied basal layer with transient excess pore pressure and laminar behaviour. Deceleration of the flow and subsequent dissipation of the pore pressure, during and after deposition of sediments, gradually remobilises the sediments to produce a patchy texture.

SM2 and SL2 facies in distal and medial sections. The internal character is thought to relate to generation and propagation of internal waves away from the confining topography as discussed previously (Fig. 14). The bed profiles and poorly sorted nature of deposits indicate that the flows were highly efficient, capable of traversing the length of the sub-basin with much of its sediment load still in suspension prior to encountering the confining topography (Gladstone et al., 1998; Salaheldin et al., 2000). The resulting interaction creates an upstream migrating sediment-bearing suspension cloud (Edwards et al., 1994; Lamb et al., 2004; Lamb et al., 2006; Toniolo et al., 2006; Patacci et al., 2015). If surge-type turbidity currents are involved in their development, as is likely to be the case here, the suspension cloud migrates upstream before breaking into a series of internal waves (Edwards et al., 1994; Tinterri et al., 2016). The initial development of the suspension cloud corresponds to increased sediment concentrations and consequently higher sediment fallout rate (Muzzi Magalhaes and Tinterri, 2010; Patacci et al., 2015; Tinterri et al., 2016). This in turn could cause the gravitational transformation of the flow in distal location to produce massive sandstones. The upstream passage of the internal waves leads to subtle fluctuations in velocity and sediment concentrations, which in turn modulates the sediment fallout rate to the static bed. The physical expression of this will be the sequence of repetitive intervals seen in facies tract III. Analogue bed character are also seen in the vicinity of onlap surfaces in the Tabernas Basin of SE Spain and the Piedmont Basin of NW Italy (Haughton, 2000; Felletti, 2002). These basins are relatively small and comparable in size to Peïra Cava sub-basin, which likely makes it easier to develop and sustain a suspension cloud to reconcentrate the flow in distal locations. In addition to the repetitive sequence described here, the generation of a suspension cloud and internal waves is also reported by Tinterri et al. (2016) and Cunha et al. (2017) as the cause of convolute lamination, load structures and diffuse soft-sediment deformation in beds in the same distal section (i.e. NE section) of the Peïra Cava sub-basin. In this case, the passage of the crests and troughs of successive waves create pressure fluctuations and consequent liquefaction and floundering.

7. Flow evolution and deposition of massive sandstones

Based on the empirical data and the interpretation presented above, the depositional history of massive sandstone depositing flows is now summarised. The presence of multiple Type I, II and III grain size breaks in the studied beds, especially in proximal locations, indicate the flow was bi-partite and unsteady. Deposition begins from a basal dense layer and results in a granular to cobble-grained deposit. The overriding high-density turbidity current subsequently deposits coarse grained massive and thick spaced stratified sandstone intervals, creating a Type I grain size break (Stevenson et al., 2014). Deposition from the high density turbidity current initially occurs via collapse of high concentration near bed layers. When sediment fallout rates are sufficiently high to prevent reworking of the layers, a graded or ungraded massive interval is likely to form. The hindered settling and grain-to-grain interaction operating within the flow during this stage is likely to create a thickness maximum in proximal locations (Talling et al., 2007a; Malgesini et al., 2015).

As the flow velocity and concentration progressively decline, the high concentration near bed layers thin and are reworked by traction to form graded, thin spaced stratified intervals. Ultimately, the declining concentration results in deposition of low density turbidites (parallel

laminated and rippled sandstone intervals) at the top of the bed, with the transition marked by a Type II grain size break. Multiple surges are likely to create a repetition of the high and low density turbidites, separated by Type II and III grain size breaks. Further downslope, the flow organises itself into a simple waning flow (Kneller and McCaffrey, 2003; Ho et al., 2018).

As the flow travels to medial sections, depositional phases are still similar to proximal locations for facies tract I and II. Bed thickness also gradually decrease to resemble a linear to crudely concave up profile. An increase in the relative proportion of massive sandstone, and a decrease in the structured facies, suggests the flow maintained its concentrations downslope, and hindered settling and grain-to-grain interaction processes continued to operate near the base of the flow. Further downslope in distal sections, flow transformation due to increased vertical stratification and turbulence suppression (facies tract I) or increased clay concentration (facies tract II) results in continued massive sandstone deposition. The presence and attrition of mud clasts likely dictates the evolution of the flow at this stage. The clasts are eroded from the muddy substrate and the amount of mud released into the flow will control the nature of the flow transformation and deposition of massive sandstone facies (Li et al., 2017; Fukuda and Naruse, 2020; Hizzett et al., 2020).

In facies tract III, the bed profile is relatively constant. The depositing flow is likely to be large volume and relatively efficient. Proximal locations are influenced by the initial surging state of the flow, similar to the facies tract I and II, while medial sections record the depletive phases. However, the higher efficiency of the flow leads to interaction with the distal confining slope topography, resulting in preferential deposition of thicker beds on the upstream side of the topography (Salaheldin et al., 2000; Kubo, 2004; Lamb et al., 2004, 2006). The interaction with the confining topography also generates an upstream migrating sediment-bearing suspension cloud which increases sediment concentrations, as well as internal waves that propagate upstream. The passage of these internal waves in distal and medial sections creates subtle fluctuations in flow velocity, sediment concentration, and pressure, which consequently influences sediment fall-out rates and the deposition repetitive sequences of facies (Haughton, 2000; Felletti, 2002; Muzzi Magalhaes and Tinterri, 2010; Tinterri and Muzzi Magalhaes, 2011; Tinterri et al., 2016; Cunha et al., 2017).

8. Conclusions

The deep-water deposits within the Peïra Cava sub-basin provide an opportunity to investigate the influence of the confining topography on bed-scale architecture. In this study, eight laterally extensive beds were investigated to document the vertical and lateral distribution of massive sandstone facies, and thus their depositional mechanisms. The eight beds contain three types of massive sandstone facies: graded massive sandstone, ungraded massive sandstone and massive sandstone with patchy texture. Statistical analysis of the internal architecture of the eight beds reveal the constituent facies are non-random, but also non-cyclic. Each facies within the bed exhibits a level of dependence on the preceding facies and exerts some influence on the succeeding facies. Thus, the vertical organisation of the internal facies is used to infer depositional processes for the three massive sandstone facies. The graded and ungraded massive sandstone facies are interpreted as deposits of high-concentration near bed layers beneath surge-type turbidity currents. These layers are characterised by hindered settling, grain to grain interaction and frictional freezing from the base up. Deposition is capacity driven since the poorly sorted nature indicates size segregation of grains was inhibited in the near bed layers. The ungraded intervals are likely to be deposited where concentrations exceed a limiting value (45% based on experimental studies) in the near bed layers, which completely suppress turbulence and grain segregation, and allow frictional interlocking of grains. In contrast, the massive sandstones with patchy texture are here interpreted to be deposits of liquefied debris flows. Dissipation of excess pore pressure via slow convection and elutriation during transit and deposition results in remobilisation of sediments, creating the 'patchy' texture.

In all eight beds, the core of the bed in proximal sections is composed of massive sandstone facies, encased by conglomeratic facies and structured sandstones at the base and top, respectively. Deposition took place from an unsteady, depletive flow with multiple surges that produced multiple grain size breaks. The vertical distribution of four types of grain size breaks (Type I to IV) indicates that the overall deposit structure in proximal sections preserves the vertical structure of a bipartite flow, with an underlying debris flow and an overlying high concentration but turbulent layer. The reduced abundance and a diversity of grain size breaks in distal sections suggests the flow evolved into a simple surge structure. Moving downslope, three facies tracts are recognised. Facies tract I and II contains predominantly ungraded massive sandstones and massive sandstone with patchy texture in distal locations, respectively. While facies tract III contains repetitive sequence of ungraded and graded massive sandstones in distal locations. This downslope transition to predominantly massive sandstone facies distally is inconsistent with existing models and observations from many ancient deposits, and is here interpreted as a record of flow interaction with the confining topography. The deposition of ungraded massive sandstones in distal locations of facies tract I is likely induced by gravity transformation of the flow as it decelerated due to an increase in slope angle. In contrast, massive sandstones with patchy texture in distal locations of facies tract II likely result from body transformation of a turbulent flow into one with a liquefied basal layer characterised by transient excess pore pressure and laminar behaviour. Such a transformation is likely modulated by a combination of incorporation and disaggregation of mud clasts, and change in slope angle. And lastly, the repetitive sequences of ungraded and graded massive sandstones in facies tract III likely result from internal waves generated as the flow deflected and reflected off confining topography. Subtle variations in flow velocity and sediment fallout rates associated with the passage of these waves create the condition necessary to deposit graded and ungraded massive sandstones.

Supplementary data to this article can be found online at https://doi.org/10.1016/j.sedgeo.2021.106001.

Declaration of competing interest

The authors declare that they have no known competing financial interests or personal relationships that could have appeared to influence the work reported in this paper.

Acknowledgements

This work was funded through the Heriot-Watt University Institute of GeoEnergy Engineering PhD scholarship. The authors would like to thank Lawrence Amy (University College Dublin) for his helpful advice on bed selection in France. We thank John and Henry Turner at T-Section Laboratories Limited for producing thin sections used in this study. Lastly, we thank the reviewers for their constructive comments on an earlier verision of the manuscript.

References

Aas, T.E., Howell, J.A., Janocko, M., Midtkandal, I., 2010. Re-created early Oligocene seabed bathymetry and process-based simulations of the Peïra Cava turbidite system. Journal of the Geological Society 167, 857–875.

Allen, J.R.L., 1982. Sedimentary structures: their character and physical basis. Development In Sedimentology. Elsevier Scientific Publishing Company 663 pp.

Amy, L.A., 2000. Architectural Analysis of a Sand-rich Confined Turbidite Basin: The Grès de Peïra Cava, South-East France. Ph.D thesisUniversity of Leeds 233pp.

Amy, L.A., Talling, P.J., 2006. Anatomy of turbidites and linked debrites based on long distance (120× 30 km) bed correlation, Marnoso Arenacea Formation, Northern Apennines, Italy. Sedimentology 53, 161–212.

Amy, L.A., McCaffrey, W.D., Kneller, B.C., 2004. The influence of a lateral basin-slope on the depositional patterns of natural and experimental turbidity currents. Geological Society, London, Special Publications 221, 311–330.

Amy, L.A., Talling, P.J., Peakall, J., Wynn, R.B., Arzola Thynne, R.G., 2005. Bed geometry used to test recognition criteria of turbidites and (sandy) debrites. Sedimentary Geology 179, 163–174.

Amy, L.A., Talling, P.J., Edmonds, V.O., Sumner, E.J., Lesueur, A., 2006. An experimental investigation of sand–mud suspension settling behaviour: implications for bimodal mud contents of submarine flow deposits. Sedimentology 53, 1411–1434.

Amy, L.A., Kneller, B.C., McCaffrey, W.D., 2007. Facies architecture of the Grés de Peira Cava, SE France: landward stacking patterns in ponded turbiditic basins. Journal of the Geological Society 164, 143–162.

Apps, G.M., 1987. The Evolution of the Grès d'Annot Basin, S.W. Alps. Ph.D thesisUniversity Of Liverpool 432pp.

Arnott, R.W.C., Hand, B.M., 1989. Bedforms, primary structures and grain fabric in the presence of suspended sediment rain. Journal of Sedimentary Research 59, 1062–1069.

Baas, J.H., 1999. An empirical model for the development and equilibrium morphology of current ripples in fine sand. Sedimentology 46, 123–138.

Baas, J.H., Best, J.L., 2002. Turbulence modulation in clay-rich sediment-laden flows and some implications for sediment deposition. Journal of Sedimentary Research 72, 336–340.

Baas, J.H., Van Kesteren, W., Postma, G., 2004. Deposits of depletive high-density turbidity currents: a flume analogue of bed geometry, structure and texture. Sedimentology 51, 1053–1088.

Baas, J.H., Best, J.L., Peakall, J., Wang, M., 2009. A phase diagram for turbulent, transitional, and laminar clay suspension flows. Journal of Sedimentary Research 79, 162–183.

Baas, J.H., Best, J.L., Peakall, J., 2011. Depositional processes, bedform development and hybrid bed formation in rapidly decelerated cohesive (mud–sand) sediment flows. Sedimentology 58, 1953–1987.

Baas, J.H., Manica, R., Puhl, E., Verhagen, I., Borges, A.L.D.O., 2014. Processes and products of turbidity currents entering soft muddy substrates. Geology 42, 371–374.

Baas, J.H., Manica, R., Puhl, E., De Oliveira Borges, A.L., 2016. Thresholds of intrabed flow and other interactions of turbidity currents with soft muddy substrates. Sedimentology 63, 2002–2036.

Bouma, A.H., 1962. Sedimentology of Some Flysch Deposits: A Graphic Approach to Facies Interpretation. Ph.D thesisUniversity of Utrecht, Utrecht 162pp.

Breien, H., De Blasio, F.V., Elverhøi, A., Nystuen, J.P., Harbitz, C.B., 2010. Transport mechanisms of sand in deep-marine environments—insights based on laboratory experiments. Journal of Sedimentary Research 80, 975–990.

Cantero, M.I, Balachandar, S., Cantelli, A., Pirmez, C., Parker, G., 2009. Turbidity current with a roof: direct numerical simulation of self-stratified turbulent channel flow driven by suspended sediment. Journal of Geophysical Research 114 (C3). https://doi.org/10.1029/10.1029/2008JC004978.

Cantero, M.I., Cantelli, A., Pirmez, C., Balachandar, S., Mohrig, D., Hickson, T.A., Yeh, T.H., Naruse, H., Parker, G., 2012a. Emplacement of massive turbidites linked to extinction of turbulence in turbidity currents. Nature Geoscience 5, 42–45.

Cantero, M.I., Balachandar, S., Cantelli, A., Pirmez, C., Parker, G., 2012b. Turbidity current with a roof: direct numerical simulation of self-stratified turbulent channel flow driven by suspended sediment. Journal of Geophysical Research 114, C03008.

Cartigny, M.J.B., Eggenhuisen, J.T., Hansen, E.W.M., Postma, G., 2013. Concentration-dependent flow stratification in experimental high-density turbidity currents and their relevance to turbidite facies models. Journal of Sedimentary Research 83, 1047–1065.

Cunha, R.S., Tinterri, R., Magalhaes, P.M., 2017. Annot Sandstone in the Peïra Cava basin: an example of an asymmetric facies distribution in a confined turbidite system (SE France). Marine and Petroleum Geology 87, 60–79.

Dade, W.B., Lister, J.R., Huppert, H.E., 1994. Fine-sediment deposition from gravity surges on uniform slopes. Journal of Sedimentary Research 64, 423–432.

Davis, C., Haughton, P., McCaffrey, W.D, Scott, E., Hogg, N., Kitching, D., 2009. Character and distribution of hybrid sediment gravity flow deposits from the outer Forties Fan, Palaeocene Central North Sea, UKCS. Marine and Petroleum Geology 26, 1919–1939.

Dorrell, R.M., Hogg, A.J., Sumner, E.J., Talling, P.J., 2011. The structure of the deposit produced by sedimentation of polydisperse suspensions. Journal of Geophysical Research - Earth Surface 116, 1–12.

Dorrell, R.M., Hogg, A.J., Pritchard, D., 2013. Polydisperse suspensions: erosion, deposition, and flow capacity. Journal of Geophysical Research - Earth Surface 118, 1939–1955.

Edwards, D.A., Leeder, M.R., Best, J.L., Pantin, H.M., 1994. On experimental reflected density currents and the interpretation of certain turbidites. Sedimentology 41, 437–461.

Elliott, T., Apps, G.M., Davies, H., Evans, M., Ghibaudo, G., Graham, R.H., 1985. Field Excursion B: A Structural and Sedimentological Traverse Through the Tertiary Foreland Basin of the External Alps of South-East France. Field Excursion Guide Book. International Association Of Sedimentologist.

Felletti, F., 2002. Complex bedding geometries and facies associations of the turbiditic fill of a confined basin in a transpressive setting (Castagnola Fm., Tertiary Piedmont Basin, NW Italy). Sedimentology 49, 645–667.

Folk, R.L., Ward, W.C., 1957. Brazos river bar: a study in the significance of grain size parameters. Journal of Sedimentary Research 27, 3–26.

Fukuda, S., Naruse, H., 2020. Shape difference of mud clasts depending on depositional facies: application of newly modified elliptical fourier analysis to hybrid event beds. Journal of Sedimentary Research 90, 1410–1435.

Gladstone, C., Sparks, R.S.J., 2002. The significance of grain-size breaks in turbidites and pyroclastic density current deposits. Journal of Sedimentary Research 72, 182–191.

Gladstone, C., Phillips, J.C., Sparks, R.S.J., 1998. Experiments on bidisperse, constant-volume gravity currents: propagation and sediment deposition. Sedimentology 45, 833–843.

Hattori, I., 1976. Entropy in Markov chains and discrimination of cyclic patterns in lithologic successions. Journal of the International Association for Mathematical Geology 8, 477–497.

Haughton, P., Davis, C., McCaffrey, W.D., Barker, S., 2009. Hybrid sediment gravity flow deposits – classification, origin and significance. Marine and Petroleum Geology 26, 1900–1918.

Haughton, P.D.W., 1994. Deposits of deflected and ponded turbidity currents, Sorbas basin, South East Spain. Journal of Sedimentary Research 64, 233–246.

Haughton, P.D.W., 2000. Evolving turbidite systems on a deforming basin floor, Tabernas, SE Spain. Sedimentology 47, 497–518.

Hilton, V.C., 1994. Architecture of Deep-marine confined sandstone bodies Eocene-Oligocene Grès d'Annot Formation SE France. Ph.D thesisUniversity of Leicester 329 pp.

Hirayama, J., Nakajima, T., 1977. Analytical study of turbidites, Otadai Formation, Boso peninsula, Japan. Sedimentology 24, 747–779.

Hiscott, R.N., 1994a. Loss of capacity, not competence, as the fundamental process governing deposition from turbidity currents. Journal of Sedimentary Research 64, 209–214.

Hiscott, R.N., 1994b. Traction-carpet stratification in turbidites-fact or fiction? Journal of Sedimentary Research 64, 204–208.

Hiscott, R.N., Middleton, G.V., 1979. Depositional mechanics of thick-bedded sandstones at the base of a submarine slope, Tourelle Formation (lower Ordovcian), Quebec, Canada. In: Doyle, L.J., Pilkey, O.H. (Eds.), Geology of Continental Slopes. 27. Society of Economist, Paleontologists and Mineralogists Special Publication, pp. 307–326.

Hizzett, J.L., Sumner, E.J., Cartigny, M.J.B., Clare, M.A., 2020. Mud-clast armoring and its implications for turbidite systems. Journal of Sedimentary Research 90, 687–700.

Ho, V.L., Dorrell, R.M., Keevil, G.M., Burns, A.D., McCaffrey, W.D., 2018. Pulse propagation in turbidity currents. Sedimentology 65, 620–637.

Ilstad, T., Marr, J.G., Elverhøi, A., Harbitz, C.B., 2004. Laboratory studies of subaqueous debris flows by measurements of pore-fluid pressure and total stress. Marine Geology 213, 403–414.

Ito, M., 2008. Downfan transformation from turbidity currents to debris flows at a channel-to-lobe transitional zone: the Lower Pleistocene Otadai Formation, Boso Peninsula, Japan. Journal of Sedimentary Research 78, 668–682.

Ivaldi, J.P., 1974. Origines des material detritique des series Grès d'Annot D'apres leas donnees de la thermoluminescence. Geol. Alpine 50, 75–98.

Iverson, R.M., 1997. The physics of debris flows. Reviews of Geophysics 35, 245–296.

Joseph, P., Lomas, S.A., 2004. Deep-water sedimentation in the Alpine Foreland Basin of SE France: new perspectives on the Grès d'Annot and related systems—an introduction. Geological Society, London, Special Publications 221, 1.

Kaitna, R., Palucis, M.C., Yohannes, B., Hill, K.M., Dietrich, W.E., 2016. Effects of coarse grain size distribution and fine particle content on pore fluid pressure and shear behaviour in experimental debris flows. Journal of Geophysical Research - Earth Surface 121, 415–441.

Kane, I.A., Pontén, A.S.M., 2012. Submarine transitional flow deposits in the Paleogene Gulf of Mexico. Geology 40, 1119–1122.

Kane, I.A., Kneller, B.C., Dykstra, M., Kassem, A., McCaffrey, W.D., 2007. Anatomy of a submarine channel–levee: an example from upper cretaceous slope sediments, Rosario Formation, Baja California, Mexico. Marine and Petroleum Geology 24, 540–563.

Kneller, B., 1995. Beyond the turbidite paradigm: physical models for deposition of turbidites and their implications for reservoir prediction. Geological Society, London, Special Publications 94, 31–49.

Kneller, B., McCaffrey, W.D., 1999. Depositional effects of flow nonuniformity and stratification within turbidity currents approaching a bounding slope; deflection, reflection, and facies variation. Journal of Sedimentary Research 69, 980–991.

Kneller, B.C., Branney, M.J., 1995. Sustained high-density turbidity currents and the deposition of thick massive sands. Sedimentology 42, 607–616.

Kneller, B.C., McCaffrey, W., 2003. The interpretation of vertical sequences in turbidite beds: the influence of longitudinal flow structure. Journal of Sedimentary Research 73, 706–713.

Kneller, B.C., Edwards, D., McCaffrey, W.D., Moore, R., 1991. Oblique reflection of turbidity currents. Geology 19, 250–252.

Kubo, Y., 2004. Experimental and numerical study of topographic effects on deposition from two-dimensional, particle-driven density currents. Sedimentary Geology 164, 311–326. https://doi.org/10.1016/j.sedgeo.2003.11.002.

Lamb, M.P., Hickson, T., Marr, J.G., Sheets, B., Paola, C., Parker, G., 2004. Surging versus continuous turbidity currents: flow dynamics and deposits in an experimental intraslope mini basin. Journal of Sedimentary Research 74, 148–155.

Lamb, M.P., Toniolo, H., Parker, G., 2006. Trapping of sustained turbidity currents by intraslope mini basins. Sedimentology 53, 147–160.

Leclair, S.F, Arnott, R.W.C, 2005. Parallel lamination formed by high density turbidity currents. Journal of Sedimentary Research 75, 1–5. https://doi.org/10.2110/jsr.2005.001.

Lee, S.E., Amy, L.A., Talling, P.J., 2004. The character and origin of thick base-of-slope sandstone units of the Peïra Cava outlier, SE France. Geological Society, London, Special Publications 221, 331–347.

Li, S., Li, S., Shan, X., Gong, C., Yu, X., 2017. Classification, formation, and transport mechanisms of mud clasts. International Geology Review 1–12.

Lowe, D.R., 1976. Subaqueous liquefied and fluidized sediment flows and their deposits. Sedimentology 23, 285–308.

Lowe, D.R., 1982. Sediment gravity flows: II depositional models with special reference to the deposits of high-density turbidity currents. Journal of Sedimentary Research 52, 279–297.

Macdonald, D.I.M., 1986. Proximal to distal sedimentological variation in a linear turbidite trough: implications for the fan model. Sedimentology 33, 243–259.

Major, J.J., 2000. Gravity-driven consolidation of granular slurries–implications for debris-flow deposition and deposit characteristics. Journal of Sedimentary Research 70, 64–83.
Major, J.J., Iverson, R.M., 1999. Debris-flow deposition: effects of pore-fluid pressure and friction concentrated at flow margins. Geological Society of America Bulletin 111, 1424–1434.
Malgesini, G., Talling, P.J., Hogg, A.J., Armitage, D., Goater, A., Felletti, F., 2015. Quantitative analysis of submarine-flow deposit shape in the Marnoso-Arenacea Formation: what is the signature of hindered settling from dense near-bed layers? Journal of Sedimentary Research 85, 170–191.
Marr, J.G., Harff, P.A., Shanmugam, G., Parker, G., 2001. Experiments on subaqueous sandy gravity flows: the role of clay and water content in flow dynamics and depositional structures. Geological Society of America Bulletin 113, 1377–1386.
McCaffrey, W.D., Kneller, B., 2001. Process controls on the development of stratigraphic trap potential on the margins of confined turbidite systems and aids to reservoir evaluation. American Association of Petroleum Geologists Bulletin 85, 971–988.
Mcintosh, C.K., 2007. The Controls on Sedimentation and Implication for Facies Prediction in the Buzzard Feld, UK North Sea. Ph.D thesisHeriot-Watt University, Edinburgh 320 pp.
Mulder, T., Alexander, J., 2001. The physical character of subaqueous sedimentary density flows and their deposits. Sedimentology 48, 269–299.
Mutti, E., 1992. Turbidite Sandstones. Istituto di Geologia Università di Parma and AGIP. Milanese, San Donato 275 pp.
Mutti, E., Tinterri, R., Remacha, E., Mavilla, N., Angella, S., Fava, L., 1999. An Introduction to the Analysis of Ancient Turbidite Basins From an Outcrop Perspective. AAPG Continuing Education Course Notes Series39 93 pp.
Mutti, E., Tinterri, R., Benevelli, G., Biase, D.D., Cavanna, G., 2003. Deltaic, mixed and turbidite sedimentation of ancient foreland basins. Marine and Petroleum Geology 20, 733–755.
Muzzi Magalhaes, P., Tinterri, R., 2010. Stratigraphy and depositional setting of slurry and contained (reflected) beds in the Marnoso-arenacea formation (Langhian-Serravallian) Northern Apennines, Italty. Sedimentology 57, 1685–1720. https://doi.org/10.1111/j.1365-3091.2010.01160.x.
Nemec, W., 1995. The dynamics of deltaic suspension plumes. In: Oti, M.N., Postma, G. (Eds.), Geology of Deltas. A.A. Balkema, Rotterdam, pp. 31–93.
Pantin, H.M., Leeder, M.R., 1987. Reverse flow in turbidity currents: the role of internal solitons. Sedimentology 34, 1143–1155.
Patacci, M., Haughton, P.D.W., McCaffrey, W.D., 2014. Rheological complexity in sediment gravity flows forced to decelerate against a confining slope, Braux, SE France. Journal of Sedimentary Research 84, 270–277.
Patacci, M., Haughton, P.D.W., McCaffrey, W.D., 2015. Flow behaviour of ponded turbidity currents. Journal of Sedimentary Research 85, 885–902.
Patel, U.S., 2018. Deep Water Massive Sands: Grain to Depositional Element Scale Analysis of Their Internal Character. Ph.D thesisHeriot-Watt University, Edinburgh 300pp.
Pickering, K.T., Hilton, V.C., 1998. Turbidite Systems of Southeast France: Application to Hydrocarbon Prospectivity. Vallis Press, London 229 pp.
Pickering, K.T., Hiscott, R.N., 2015. Deep Marine Systems: Processes, Deposits, Environments, Tectonics And Sedimentation. John Wiley & Sons Ltd, Oxford 658pp.
Piper, D.J.W., 1978. Turbidite muds and silts on deep sea fans and abyssal plains. In: Stanley, D.J., Kelling, G. (Eds.), Sedimentation in Submarine Canyons, Fans and Trenches. Dowden, Hutchinson and Ross, Stroudsburg, Pennsylvania, pp. 163–271.
Piper, D.J.W., Cochonat, P., Morrison, M.L., 1999. The sequence of events around the epicentre of the 1929 grand banks earthquake: initiation of debris flows and turbidity current inferred from sidescan sonar. Sedimentology 46, 79–97.
Plink-Björklund, P., Steel, R.J., 2004. Initiation of turbidity currents: outcrop evidence for Eocene hyperpycnal flow turbidites. Sedimentary Geology 165, 29–52.
Pochat, S., Van den Driessche, J., 2007. Impact of synsedimentary metre-scale normal fault scarps on sediment gravity flow dynamics: an example from the Grès d'Annot Formation, SE France. Sedimentary Geology 202, 796–820.
Postma, G., Nemec, W., Kleinspehn, K.L., 1988. Large floating clasts in turbidites: a mechanism for their emplacement. Sedimentary Geology 58, 47–61.
Powers, D.W., Easterling, R.G., 1982. Improved methodology for using embedded Markov chains to describe cyclical sediments. Journal of Sedimentary Research 52, 913–923.
Ravenne, C., Vially, R., Richié, P., Trémolières, P., 1987. Sédimentation et tectonique dans le basin marine Éocene supérieur – Oligocène des Alpes du sud. Revue de l'institut Français de Pétrole 42, 529–553.
Remacha, E., Ferandez, L.P., Maestro, E., 2005. The transition between sheet-like lobe and basin plain turbidites in the Hecho Basin (South-Central Pyrenees, Spain). Journal of Sedimentary Research 75, 798–819.
Salaheldin, T.M., Imran, J., Chaudhry, M.H., Reed, C., 2000. Role of fine-grained sediment in turbidity current flow dynamics and resulting deposits. Marine Geology 171, 21–38.
Sanders, J.E., 1965. Primary sedimentary structures formed by turbidity currents and related resedimentation mechanisms. In: Middleton, G.V. (Ed.), Primary Sedimentary Structures and Their Hydrodynamic Interpretation. Society of Economic Palaeontologists and Mineralogists Special Publications, pp. 192–219.
Shanmugam, G., 1996. High-density turbidity currents: are they sandy debris flows? Journal of Sedimentary Research 66, 2–10.
Sinclair, H.D., 1994. The influence of lateral basinal slopes on turbidite sedimentation in the Annot Sandstones of SE France. Journal of Sedimentary Research 64, 42–54.
Sinclair, H.D., 2000. Deltas-fed turbidites infilling a topographically complex basin: a new depositional model for the Annot Sandstones, SE France. Journal of Sedimentary Research 70, 504–519.
Sinclair, H.D., Cowie, P.A., 2003. Basin-floor topography and the scaling of turbidites. Journal of Geology 111, 277–299.
Sinclair, H.D., Tomasso, M., 2002. Depositional evolution of intra-slope turbidite subbasins. Journal of Sedimentary Research 72, 452–457.
Sohn, Y.K., 1997. On traction-carpet sedimentation. Journal of Sedimentary Research 67, 502–509.
Stanley, D.J., Palmer, H.D., Dill, R.F., 1978. Coarse sediment transport by mass flow and turbidity current processes and downslope transformations in Annot Sandstone canyon-fan valley systems. In: Stanley, D.J., Kelling, G. (Eds.), Sedimentation, Submarine Canyons, Fan, and Trenches. Dowden, Hutchinson and Ross, Stroudsburg PA, pp. 85–113.
Steel, E., Buttles, J., Simms, A.R., Mohrig, D., Meiburg, E., 2017. The role of buoyancy reversal in turbidite deposition and submarine fan geometry. Geology 45, 35–38.
Stevenson, C.J., Peakall, J., 2010. Effects of topography on lofting gravity flows: implications for the deposition of deep-water massive sands. Marine and Petroleum Geology 27, 1366–1378.
Stevenson, C.J., Talling, P.J., Masson, D.G., Sumner, E.J., Frenz, M., Wynn, R.B., 2014. The spatial and temporal distribution of grain-size breaks in turbidites. Sedimentology 61, 1120–1156.
Stow, D.A.V., Johansson, M., 2000. Deep-water massive sands: nature, origin and hydrocarbon implications. Marine and Petroleum Geology 17, 145–174.
Sumner, E.J., Amy, L.A., Talling, P.J., 2008. Deposit structure and processes of sand deposition from decelerating sediment suspensions. Journal of Sedimentary Research 78, 529–547.
Sumner, E.J., Talling, P.J., Amy, L.A., 2009. Deposits of flows transitional between turbidity current and debris flow. Geology 37, 991–994.
Sumner, E.J., Talling, P.J., Amy, L.A., Wynn, R.B., Stevenson, C.J., Frenz, M., 2012. Facies architecture of individual basin-plain turbidites: comparison with existing models and implications for flow processes. Sedimentology 59, 1850–1887.
Sylvester, Z., Lowe, D.R., 2004. Textural trends in turbidites and slurry beds from the oligocene flysch of the East Carpathians, Romania. Sedimentology 51, 945–972.
Talling, P.J., Amy, L.A., Wynn, R.B., Peakall, J., Robinson, M., 2004. Beds comprising debrite sandwiched within co-genetic turbidite: origin and widespread occurrence in distal depositional environments. Sedimentology 51, 163–194.
Talling, P.J., Amy, L.A., Wynn, R.B., 2007a. New insight into the evolution of large-volume turbidity currents: comparison of turbidite shape and previous modelling results. Sedimentology 54, 737–769.
Talling, P.J., Wynn, R.B., Masson, D.G., Frenz, M., Cronin, B.T., Schiebel, R., Akhmetzhanov, A.M., Dallmeier-Tiessen, S., Benetti, S., Weaver, P.P.E., Georgiopoulou, A., Zühlsdorff, C., Amy, L.A., 2007b. Onset of submarine debris flow deposition far from original landslide. Nature Letters 450, 541–544.
Talling, P.J., Masson, D.G., Sumner, E.J., Malgesini, G., 2012. Subaqueous sediment density flows: depositional processes and deposit types. Sedimentology 59, 1937–2003.
Talling, P.J., Malgesini, G., Felletti, F., 2013. Can liquefied debris flows deposit clean sand over large areas of sea floor? Field evidence from the Marnoso-Arenacea Formation, Italian Apennines. Sedimentology 60, 720–762.
Tinterri, R., Muzzi Magalhaes, P., 2011. Synsedimentary structural control on foredeep turbidites: an example from Miocene Marnoso arenacea Formation, northern Apennines, Italy. Marine and Petroleum Geology 28, 629–657.
Tinterri, R., Piazza, A., 2019. Turbidites facies response to the morphological confinement of a foredeep (Cervarola Sandstones Formation, Miocene, northern Apennines, Italy). Sedimentology 66, 636–674.
Tinterri, R., Drago, M., Consonni, A., Davoli, G., Mutti, E., 2003. Modelling subaqueous bipartite sediment gravity flows on the basis of outcrop constraints: first results. Marine and Petroleum Geology 20, 911–933. https://doi.org/10.1016/j.marpetgeo.2003.03.003.
Tinterri, R., Muzzi Magalhaes, P., Tagliaferri, A., Cunha, R.S., 2016. Convolute laminations and load structures in turbidites as indicators of flow reflections and decelerations against bounding slopes. Examples from the Marnoso-arenacea Formation (northern Italy) and Annot Sandstones (south eastern France). Sedimentary Geology 344, 382–407.
Tinterri, R., Laporta, M., Ogata, K., 2017. Asymmetrical cross-current turbidite facies tract in a structurally-confined mini-basin (Priabonian-Rupelian, Ranzano Sandstone, northern Apennines, Italy). Sedimentary Geology 352, 63–87. https://doi.org/10.1016/j.sedgeo.2016.12.005.
Tokuhashi, S., 1989. Two stage of submarine fan sedimentation in an ancient forearc basin, central Japan. In: Taira, A., Masuda, F. (Eds.), Sedimentary Facies in the Active Plate Margin. Terra Scientific Publications, Tokyo, pp. 439–468.
Toniolo, H., Lamb, M., Parker, G., 2006. Depositional turbidity currents in diapiric minibasins on the continental slope: formulation and theory. Journal of Sedimentary Research 76, 783–797.
Vrolijk, P.J., Southard, J.B., 1997. Experiments on rapid deposition of sand from high-velocity flows. Geoscience Canada 24, 45–54.